PERFORMANCE PREDICTION OF DARRIEUS TYPE VERTICAL AXIS WIND TURBINES USING NUMERICAL SIMULATIONS

A THESIS SUBMITTED TO
THE GRADUATE SCHOOL OF NATURE AND APPLIED SCIENCE
OF
MIDDLE EAST TECHNICAL UNIVERSITY

BY

FAZIL SELÇUK GÖMEÇ

IN PARTIAL FULFILLMENT OF THE REQUIREMENTS
FOR
THE DEGREE OF MASTER OF SCIENCE
IN
MECHANICAL ENGINEERING

JANUARY 2014

Approval of thesis:

PERFORMANCE PREDICTION OF DARRIEUS TYPE VERTICAL AXIS WIND TURBINES USING NUMERICAL SIMULATIONS

submitted by **FAZIL SELÇUK GÖMEÇ** in partial fulfillment of the requirements for the degree of **Master of Science in Mechanical Engineering Department, Middle East Technical University** by,

Prof.Dr.Canan Özgen
Dean,Graduate School of **Natural and Applied Sciences** _____

Prof.Dr.Süha Oral
Head of Department, **Mechanical Engineeing** _____

Asst.Prof.Dr.Cüneyt Sert
Supervisor, **Mechanical Engineeing Dept.,METU** _____

Examining Committee Members:

Prof.Dr.Mehmet Haluk Aksel
Mechanical Engineeing Dept.,METU _____

Asst.Prof.Dr.Cüneyt Sert
Mechanical Engineeing Dept.,METU _____

Assoc.Prof.Dr.İlker Tarı
Mechanical Engineeing Dept.,METU _____

Asst.Prof.Dr.Mehmet Metin Yavuz
Mechanical Engineeing Dept.,METU _____

Assoc.Prof.Dr.Oğuz Uzol
Aerospace Engineeing Dept.,METU _____

Date: 24.01.2014

I hereby declare that all information in this document has been obtained and presented in accordance with academic rules and ethical conduct. I also declare that, as required by these rules and conduct, I have fully cited and referenced all material and results that are not original to this work.

Name, Last name : Fazıl Selçuk Gömeç

Signature:

ABSTRACT

PERFORMANCE PREDICTION OF DARRIEUS TYPE VERTICAL AXIS WIND TURBINES USING NUMERICAL SIMULATIONS

Gömeç, Fazıl Selçuk
M.S.,Department of Mechanical Engineering
Supervisor: Asst. Prof. Dr. Cüneyt Sert

January 2014, 80 pages

Flow over Darrieus type straight-bladed vertical axis wind turbines (VAWT) with NACA 0021 blade profile is simulated using ANSYS Fluent software. SST k-ω turbulence model is used for the two-dimensional, unsteady simulations. Wind speed is taken as 7 m/s and part of the problem domain including the rotating blades is modeled using the sliding mesh technique. Effects of boundary layer mesh parameters, time step and convergence tolerance on the solution accuracy are investigated with carefully designed runs. Performance of VAWTs with 2 and 3 blades, which are designed to have the same solidity ratio, are compared at different tip speed ratios. Instantaneous flow patterns of unsteady flow fields are analyzed by examining velocity and pressure contours. Start-up performance, which is known to be critical for Darrieus turbines, is investigated with special care and the effect of number of blades to this issue is studied.

Keywords: Vertical Axis Wind Turbine (VAWT), Darrieus Turbine, Computational Fluid Dynamics (CFD), Unsteady Flow Modeling

ÖZ

DARRIEUS TİPİ DİKEY EKSENLİ RÜZGAR TÜRBİNLERİNİN PERFORMANSININ SAYISAL BENZETİMLERLE TAHMİNİ

Gömeç, Fazıl Selçuk
Yüksek Lisans, Makine Mühendisliği Bölümü
Tez Yöneticisi: Yrd. Doç. Dr. Cüneyt Sert

Ocak 2014, 80 sayfa

Darrieus tipi, düz kanatlı ve NACA 0021 kanat profiline sahip dikey eksenli rüzgar türbinleri (DERT) üzerindeki akış, ANSYS-Fluent HAD yazılımı kullanılarak çözüldü. Benzetimler 2-boyutlu, zamana bağlı ve SST k-ω türbülans modeli kullanılarak 7 m/s sabit rüzgar hızı için yapıldı. Kanatların döndüğü kısmı kayan sayısal ağ olarak modellendi. Dikkatli tasarlanmış analizler sayesinde sınır tabakaya ait sayısal ağ parametrelerinin, zaman adımı ve yakınsama toleranslarının çözüm üzerindeki etkileri saptandı. Toplam kord uzunlukları aynı olacak şekilde tasarlanmış 2 ve 3 kanatlı türbinlerinin performansları farklı tip-hız oranları için elde edildi ve karşılaştırıldı. Zamana bağlı akış alanları hız ve basınç dağılım grafikleri kullanılarak incelendi. Dikey eksenli rüzgar türbinlerinde sorunlu olan başlangıç anı detaylı olarak incelendi ve kanat sayısının başlangıç problemine etkisi çalışıldı.

Anahtar Kelimeler: Dikey Eksenli Rüzgar Türbini (DERT), Darrieus Türbini, Hesaplamalı Akışkanlar Dinamiği (HAD), Zamana Bağlı Akış Modelleme

To My Lovely Family

ACKNOWLEDGEMENTS

The author wishes to express his deepest respects, appreciations and thanks to his thesis advisor Assistant Professor Dr. Cüneyt Sert for his guidance and advices on research methods and ethicals issues of engineering.

The author would also like to state his appreciations to his dear friends Salih Barış Ünal and Erçin Aydemir for their assistance and support during thesis study.

Also, the author would like to thank his lovely wife Mehtap, patient parents Demet and İsmail and hard-working brother Emre for their support and understandings at his stressful times.

TABLE OF CONTENTS

LIST OF FIGURES

FIGURES

LIST OF TABLES

TABLES

LIST OF SYMBOLS

ABBREVIATIONS

VAWT	Vertical Axis Wind Turbine
HAWT	Horizontal Axis Wind Turbine
NACA	National Advisory Commitee for Aeronautics
CFD	Computational Fluid Dynamics
RANS	Reynolds Averaged Navier-Stokes
FVM	Finite Volume Method
SST	Shear Stress Transport
TKE	Turbulent Kinetic Energy
SDR	Specific Dissipation Rate
SIMPLE	Semi Implicit Method for Pressure Linked Equations
PRESTO	Pressure Staggering Option
IEC	International Electrotechnical Commitee
FFT	Fast Fourier Transform
RMS	Root Mean Square

SYMBOLS

E	Energy extracted from the air motion (Joule)
M	Total mass of the air (kg)
V	Velocity of air (m/s)
P	Energy extracted from the air motion (J/S, Watt)
$\dot{m}$	Mass flow rate (kg/s)
ρ_a	Density of the air (kg/m^3)
TSR	Tip Speed Ratio
W	Rotational speed of the wind turbine(rad/s)
V_∞	Free stream velocity (m/s)
σ	Solidity ratio
c	Chord length of the related airfoil (m)
R	Radius of the wind turbine (m)

N	Number blades of the wind turbine
A	Projected area
H	Height of the wind turbine
D	Diameter of the wind turbine
C_m	Moment coefficient
C_P	Power coefficient
T	Torque generated by the wind turbine
V_T	Tangential velocity
V_N	Normal velocity
V_a	Induced velocity of free stream
W	Local relative flow velocity
C_T	Tangential force coefficient on the blade
F_T	Tangential force on the blade
F_{Ta}	Average tangential force on the blade
Q	Total average torque of the wind turbine
C_N	Normal force coefficient on the blade
α	Angle of attack
S	Area of flow section used in the Betz's limit
F	Force applied by the air stream on the wind turbine
b	Interference parameter of the Betz's limit
P_{TOT}	The total maximum power of the turbine

CHAPTER 1

INTRODUCTION

1.1. WIND ENERGY BASICS

For a clear understanding of the wind energy one can start by searching answers of the following questions

- Where does the wind come from?
- What is the available power of air flow?

Sources of the wind can be considered in two main groups known as pressure gradient and Coriolis effect. Pressure gradients originate from the temperature differences on the Earth surface. When the surface temperature increases, air moves up and its pressure decreases, while the opposite occurs when temperature decreases. Therefore surface temperature differences results in the motion of air from the high pressure regions to the low ones. Solar radiation is the main source of heating that causes surface temperature changes. For example consider two points on the Earth's surface, one being on the equator and the second on the North Pole. It is expected to see a wind regime between these points due to the annual temperature differences between them. Not only global climate effects, but also local ones such as daily temperature differences between the oceans, seas and lands cause surface temperature changes.

In addition to the local and global pressure gradients, the rotation of the earth has an important influence on the wind motion, known as the Coriolis effect. If the Earth's surface is assumed as a wall, the speed of the air should be equal to the Earth's speed on the surface, due to the no slip condition. In addition, the Earth's surface moves faster around the equator than around the poles, which causes different wind regimes [1] (See Fig. 1.1). Global pressure gradients combined with the Coriolis effect result in the large scale wind regimes shown in Fig. 1.2.

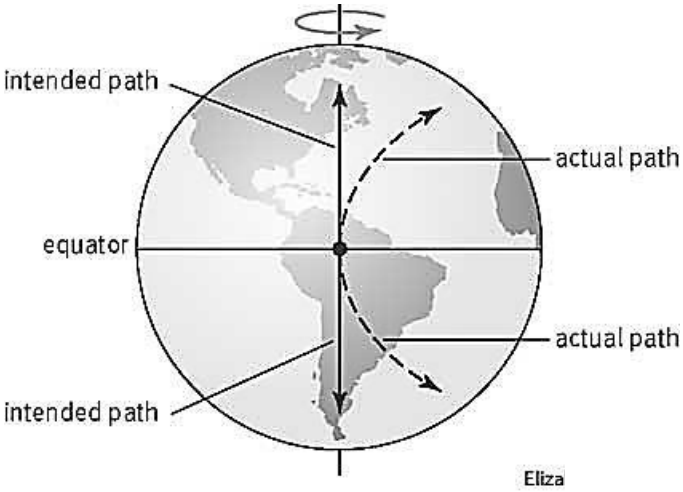

Figure 1.1. The effect of Coriolis force on wind regimes [2]

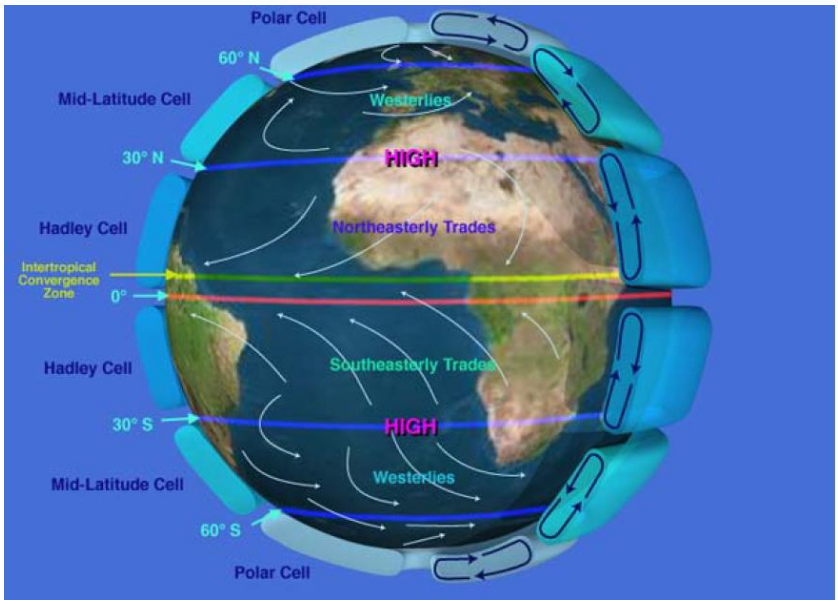

Figure 1.2. The main global wind regimes [1]

Coming to the second question, consider the available power to be the maximum power that can be converted into another form of energy. Kinetic energy of the air motion should be analyzed to reach the potential power since wind turbines are devices converting kinetic energy of moving air to the electrical energy [3]. Equation (1.1) gives the general kinetic energy relation.

$$E = \frac{1}{2} m V^2 \tag{1.1}$$

E : Energy extracted from the air motion [J]

m : Total mass of the air [kg]

V : Velocity of air [m/s]

By replacing mass with mass flow rate ($\dot{m}$), power extracted (P) can be calculated as

$$P = \frac{1}{2} \dot{m} V^2 \tag{1.2}$$

The mass flow rate of air can be written in terms of its density (ρ_a), cross sectional area (A) through which the air flows and air velocity (V) as follows.

$$\dot{m} = \rho_a A V \tag{1.3}$$

Using Eqn. (1.3) in Eqn. (1.2) we get the following relation that can be used to estimate the potential power in air flow

$$P = \frac{1}{2} \rho_a A V^3 \tag{1.4}$$

in which ($\rho_a A$) term is also known as the volumetric flow rate (Q).

1.2. WIND TURBINES

Wind turbines are devices that convert mechanical energy to electrical energy. Until the World War II their use was limited to Denmark, but later they have been gained popularity to utilize wind energy as a renewable resource [4]. After 1990s, the wind power capacity in the World has been increased rapidly. According to the statistics of the Global Wind Energy Council, total installed wind power capacity increased from 6.1 GW to 282.6 GW between 1996 and 2012 [5]. As seen in Fig. 1.3 the rate of increase of total installed wind power also increased each year. Although Turkey has great wind power potential, it started to invest in wind power mainly after 2007 as seen in Fig. 1.4 [6].

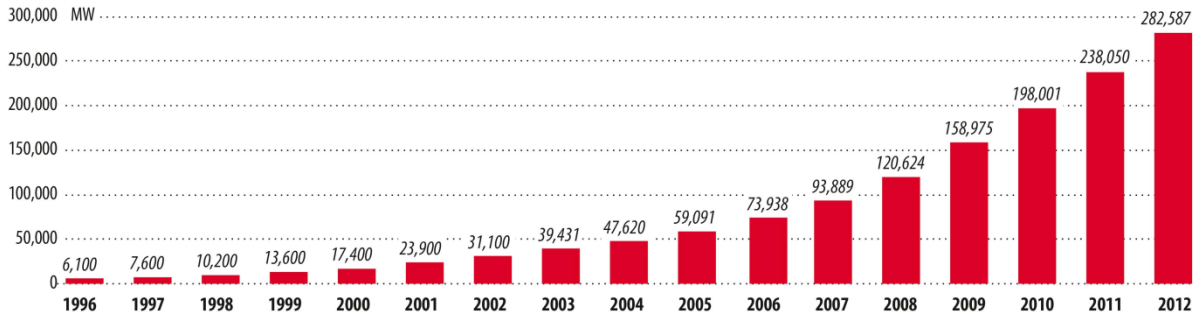

Figure 1.3. Global cumulative installed wind power capacity [5]

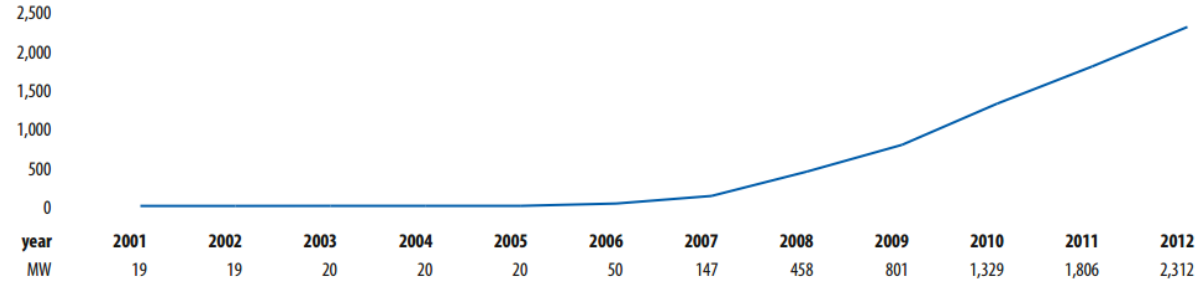

Figure 1.4. Cumulative installed wind capacity of Turkey [6]

Wind turbines are classified into two main groups as horizontal (HAWT) and vertical (VAWT) axis wind turbines. This classification is done according to the axis of rotation with respect to the air flow direction. As seen in Fig. 1.3, for HAWTs the axis of rotation is parallel to the air flow, while it is perpendicular VAWTs.

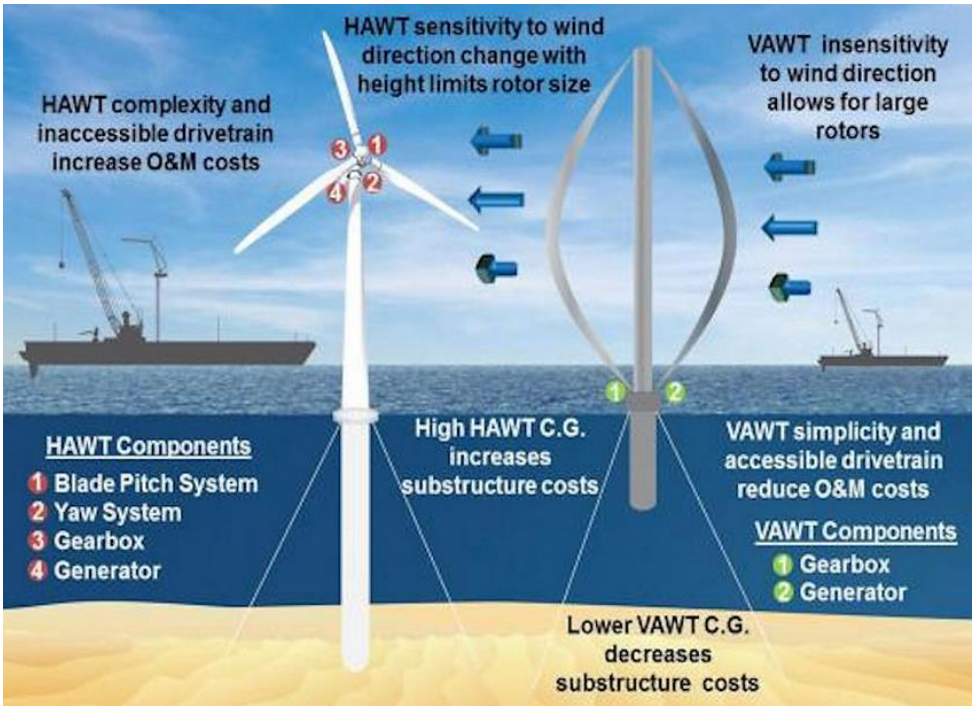

Figure 1.5. An overview to the horizontal and vertical axis wind turbines [7]

The most important difference between these two types is the dependency to the wind direction. VAWTs always rotate perpendicular to the wind, wherever it is coming from, i.e. their operation is independent of the wind direction, which is an important advantage. On the other hand wind direction is crucial for the effective operation of HAWTs. Still, HAWTs are much more popular than VAWTs in large-scale wind energy utilization, due to their installation in farms where there is a dominant wind direction and the use of specialized yawing mechanisms, which make sure that the turbines always receive the wind right from the head. But these complicated mechanisms increase manufacturing and installation costs. That's why; HAWTs lose their popularity in small-scale models. Today, VAWTs are generally used for small-scale applications with 250 – 3000 W maximum power [8, 9, 10]. This thesis also considers this power range.

With respect to the driving force, VAWTs are classified as drag driven and lift driven. Drag driven VAWTs are known as Savonius turbines. As seen in Fig. 1.6 they are driven by the air drag acting on their blades. Lift driven VAWTs are known

as Darrieus turbines. As seen in Fig. 1.7 they rotate by the torque generated by the lift force acting to their blades. To achieve this, their blades are designed as airfoil sections. Darrieus type VAWTs are known to be more efficient than Savonius types, and they are the focus of this thesis.

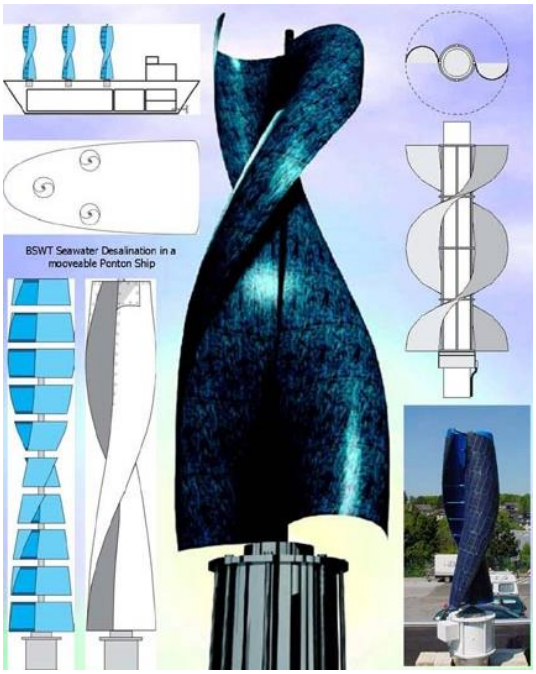

Figure 1.6. Savonius turbine [11]

Figure 1.7. Darrieus turbine [12]

1.3. AERODYNAMICS of DARRIEUS TYPE VAWTs

Definitions and equations that are necessary to understand the operation of Darrieus turbines (from now on will simply be called turbine or VAWT) are given in this section. Sketch of a 3 straight bladed Darrieus turbine is given in the Fig. 1.8. Its blades are identical, with a height of H and chord length of c. V_∞ is the free stream wind speed. The turbine rotates at a speed of ω. Independent of the wind direction, it can rotate only in one direction such that its blades receive the air from their leading edge. When seen from the top, the turbine covers a circular area of radius R, and when seen from the wind direction its projected area is HD, with $D = 2R$ being the diameter of the turbine.

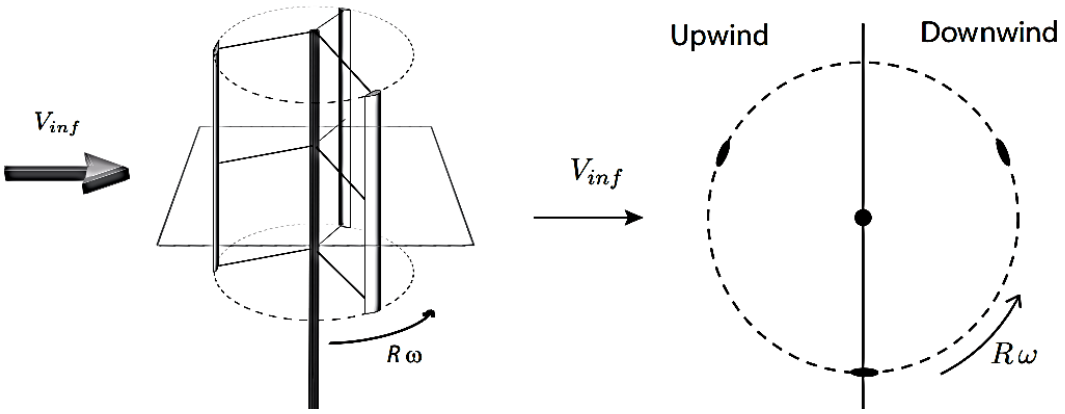

Figure 1.8. Overview of Darrieus type VAWTs [13]

Equation (1.5) combines the rotational speed of the turbine, its radius and free stream wind speed into a non-dimensional parameter known as the tip speed ratio (TSR).

$$TSR = \frac{R\omega}{V_\infty} \tag{1.5}$$

TSR is an important parameter. Overall turbine performance parameters, such as moment and power coefficients are presented with respect to this value or time dependent values of these performance parameters are calculated for a definite TSR value. In this thesis TSR values in a range of 0.15 to 4.5 are studied.

Another important non-dimensional parameter is the solidity ratio (σ), given in Eqn. (1.6). It combines the number of blades (N), chord length of each blade and the turbine radius. It is the ratio of total chord length to the radius of the turbine. It is helpful to optimize the blade chord length corresponding to the turbine radius and to compare performances of turbines with different number of blades.

$$\sigma = \frac{Nc}{R} \tag{1.6}$$

In Eqn. (1.7), the reference area that will be used in defining moment and power coefficients is based on the turbine diameter and blade height.

$$A = HD \tag{1.7}$$

Equations (1.8) and (1.9) are used to determine moment and power coefficients

$$C_m = \frac{T}{0.5\,\rho_a A V_\infty^2 R} \tag{1.8}$$

$$C_P = \frac{P}{0.5\,\rho_a A V_\infty^3} \tag{1.9}$$

where T and P are the torque and power generated by the turbine, respectively. They are related to each other through the rotational speed as given below.

$$P = T\omega \tag{1.10}$$

C_m, C_P and P are known as the performance parameters of a wind turbine.

Relationships between aerodynamic forces and turbine performance parameters are explained by Islam [10]. These equations, which will be given below, relate free stream wind speed, tangential force acting on the blade that creates the rotating torque and the generated power. To start with consider a single blade of a Darrieus turbine as shown in Fig. 1.9. Its position is determined by the azimuth angle θ. It is rotating CCW at constant speed ω in a free stream wind of speed V_∞. Induced speed V_a, is the speed of the wind as it approaches the blade. The models developed to study Darrieus turbines, details of which will be given in the next section, suggest different ways to estimate V_a. Blade's linear speed due to its rotation is ωR, which can be combined with the proper component of V_a to form the following tangential velocity (shown as cordial velocity V_c in Fig. 1.9)

$$V_T = R\omega + V_a \cos(\theta) \tag{1.11}$$

Normal velocity is related to the induced velocity as

$$V_N = V_a \sin(\theta) \tag{1.12}$$

After calculating tangential and normal velocities, the local angle of attack can be found as

$$\alpha = \tan^{-1}\left(\frac{V_N}{V_T}\right) \tag{1.13}$$

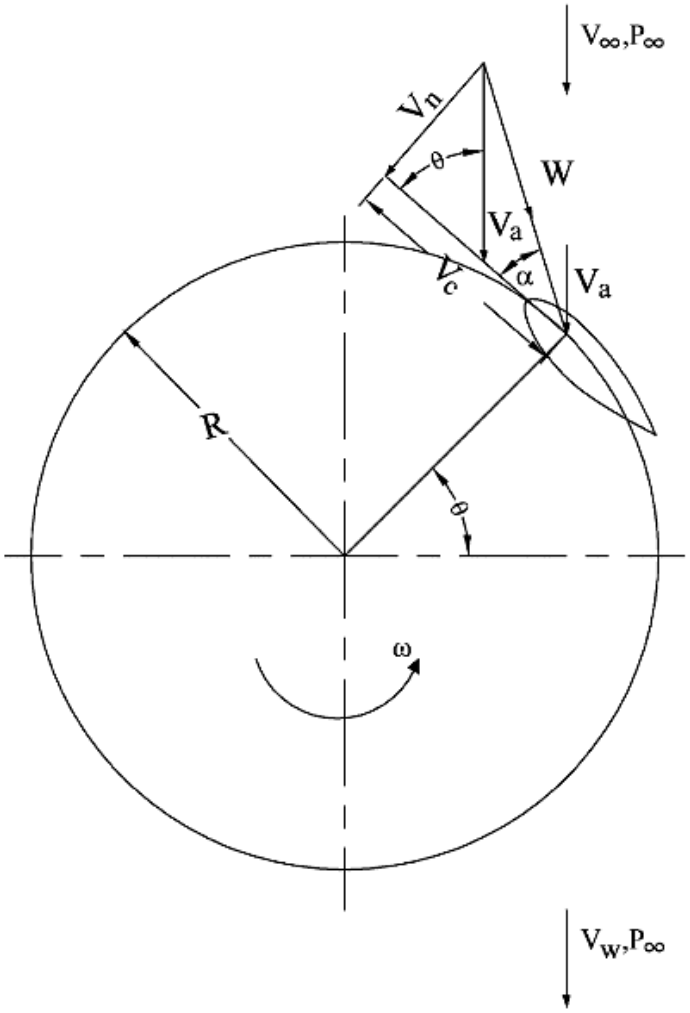

Figure 1.9. Velocity diagram for a single blade of a Darrieus turbine [14]

Another important velocity seen in Fig. 1.9 is the local relative flow velocity W, which is the vector sum of V_N and V_T.

$$W = \sqrt{V_N^2 + V_T^2} \tag{1.14}$$

It is important to find W because the lift and drag coefficients are found by the combination of it and the local angle of attack.

Knowing the airfoil geometry of the blade, relative flow velocity W and angle of attack α, lift and drag coefficients can be calculated, which can further be combined into the following tangential force coefficient

$$C_T = C_L \sin(\alpha) + C_D \cos(\alpha) \tag{1.15}$$

Tangential force that will create the required torque for rotation is given by

$$F_T = \frac{1}{2} C_T \rho_a c H W^2 \tag{1.16}$$

To reach an overall performance measure of the turbine this tangential force can be averaged over one full rotation as follows

$$\overline{F_T} = \frac{1}{2\pi} \int_0^{2\pi} F_T(\theta)\, d\theta \tag{1.17}$$

For a turbine with N blades, assuming no interaction between the blades, torque that will be created by this average force is given by

$$T = N \overline{F_T} R \tag{1.18}$$

And finally we can reach the power output of the turbine by multiplying this torque value with the rotational speed, as given by Eqn. (1.10).

In this short summary details of obtaining the induced velocity, angle of attack and lift and drag coefficients are not mentioned. In the next section different approaches used to get these values, as well as ideas to take blade interactions into account will be discussed.

1.4. MODELING APPROACHES of DARRIEUS TURBINES

In literature one can find a number of different techniques to calculate induced velocity and angle of attack. Most commonly used ones are Momentum, Vortex and Cascade models. These models are based on various simplifying assumptions and can only predict V_a and α. Lift and drag coefficients as functions of these two parameters need to be obtained from an experiment based empirical database. As done in this thesis, it is also possible to use a more advanced approach and perform a

Computational Fluid Dynamics (CFD) simulation which will give all necessary information with no simplifying assumption.

Double Multiple Stream Tube (DMST) model is one of the most widely used momentum models for performance prediction of VAWTs. Batista, Melicio, Matias and Catalao used various versions of this model for different blade geometries [15]. Beri and Yao compared this model with CFD-RANS approach and found that DMST and CFD simulations show totally different results at low tip speed ratio and small differences in power coefficients were reported at the steady state *TSR* [16]. Figure 1.10 shows Saeidi et al.'s comparison of DMST results with experimental measurements [17]. As seen for low θ values DMST model cannot predict the negative tangential force. Researchers proposed several enhancements to the DMST model, one example being the work of Goude which includes the effects of supporting struts, flow curvature and flow expansion [18].

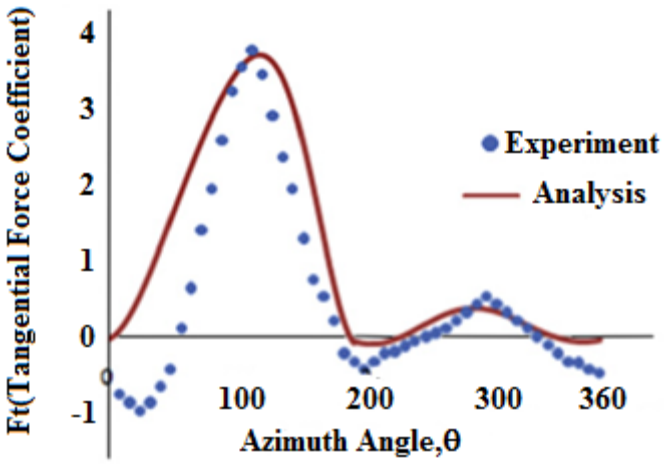

Figure 1.10. Comparison of DMST model and experimental results for Greenergy's 600W-APV-6 turbine at *TSR* = 5 [17]

Vortex models are known to be more accurate than momentum models [19]. Strickland developed a free vortex model [20], which was also used by Angle et al. [21]. Ponta and Jacovkis worked on a combination of vortex model and FEM [22] and Wang et al. proposed a less time consuming 2D vortex panel model [23]. Figure

1.11 compares the results of the vortex model developed by Dumitrescu and Cardos [24] with DMST and experimental results. As shown in the figure vortex model is clearly more accurate than DMST at the lower TSR values.

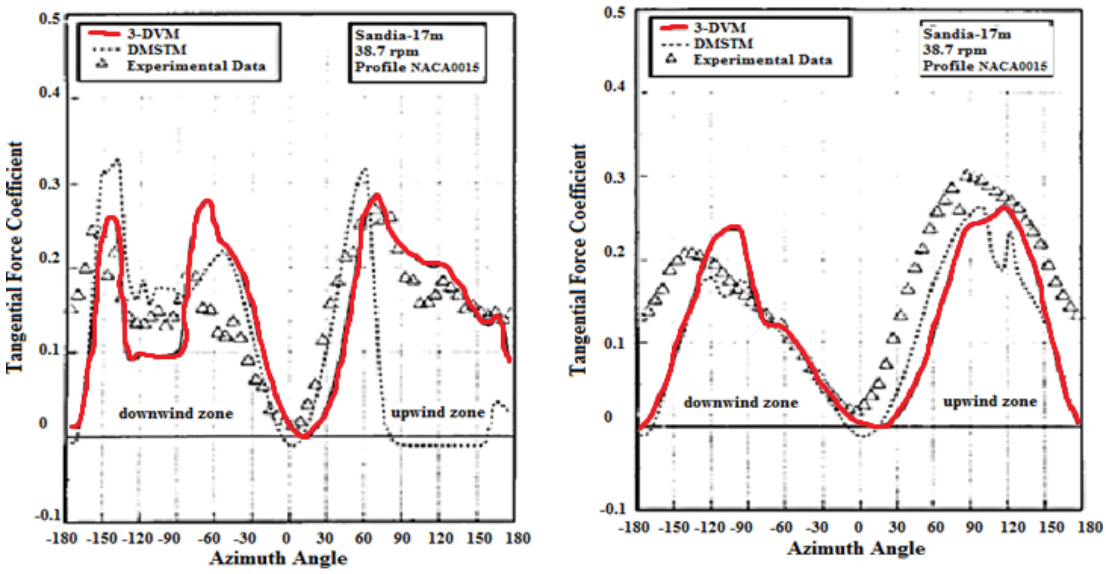

Figure 1.11. Variation of tangential force coefficient with azimuth angle for TSR 2.33 (left) and 3.7 (right) [24]

Cascade model is a popular approach for general turbo machinery design and it is also suitable to study Darrieus turbines. The technique is first applied to VAWTs by Hirsch and Mandal [25]. In this model, blades are put into a linear configuration which is called as cascade, as shown in Fig. 1.12. Fig. 1.13 compares cascade model results with two different stream tube models and experimental results, performed by Islam [26]. As seen in the figure more accurate results are obtained by the cascade model at higher tip speed ratios. In this study Islam used an improved Cascade model that takes dynamic stall, flow curvature and parasitic drag effects into account.

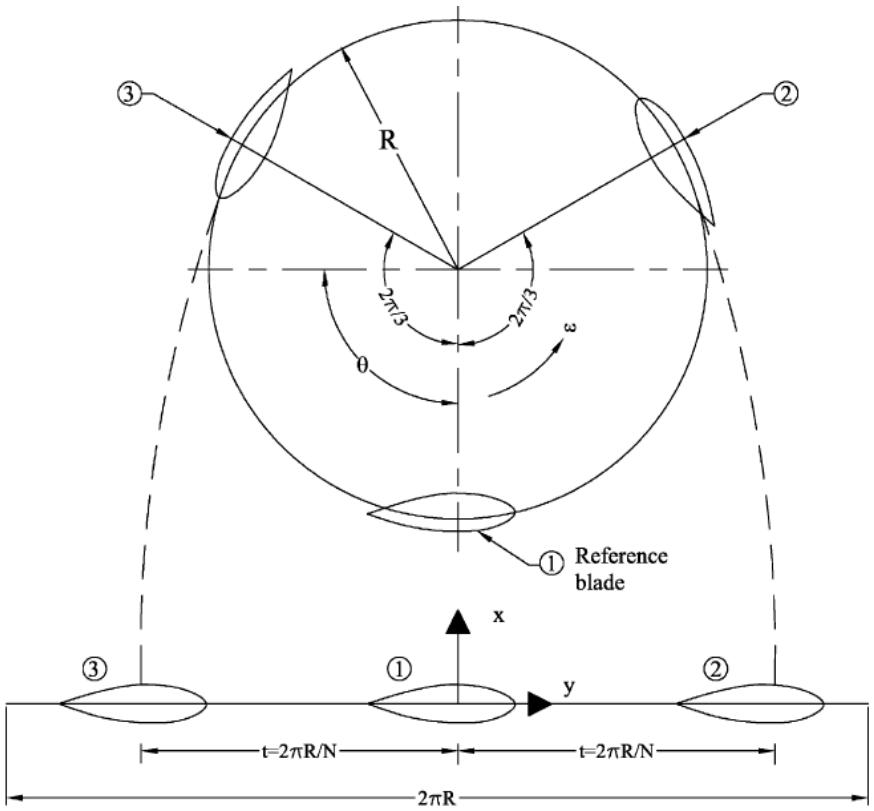

Figure 1.12. VAWT in the cascade configuration [26]

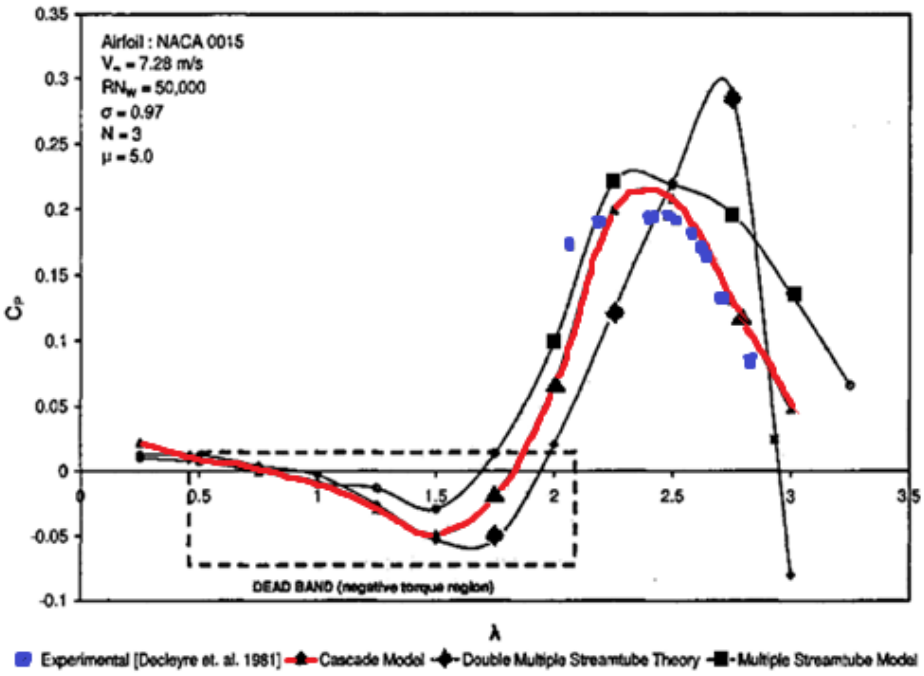

Figure 1.13. Variation of power coefficient with tip speed ratio obtained by cascade and stream tube models and experiments [26]

Models explained up to now share the same weakness of not being able to calculate lift and drag coefficients. Also to some extent they all suffer from inaccurate prediction of wake regions and therefore the interaction between the blades. Computational Fluid Dynamics (CFD) simulations are known to be superior in terms of general accuracy and they can predict lift and drag coefficients as well. Their general disadvantage compared to other models is the tedious pre-processing of the computational mesh, as well as the long run time and high level computational hardware they require, especially for 3D analyses.

The general approach to perform CFD simulation of a Darrieus turbine is known as the sliding mesh technique, for which three different mesh zones are created as shown in the Fig. 1.14. The rotating domain contains the blades. It is surrounded by the inner and outer stationary domains with sliding mesh interfaces in between. Unsteady performance characteristics of the turbine is obtained by the prescribed angular motion of the rotating domain at each time step and. The simulations are done by the solution of Navier-Stokes equations with a suitable turbulence model. Generally, finite volume method is used to discretize the governing equations.

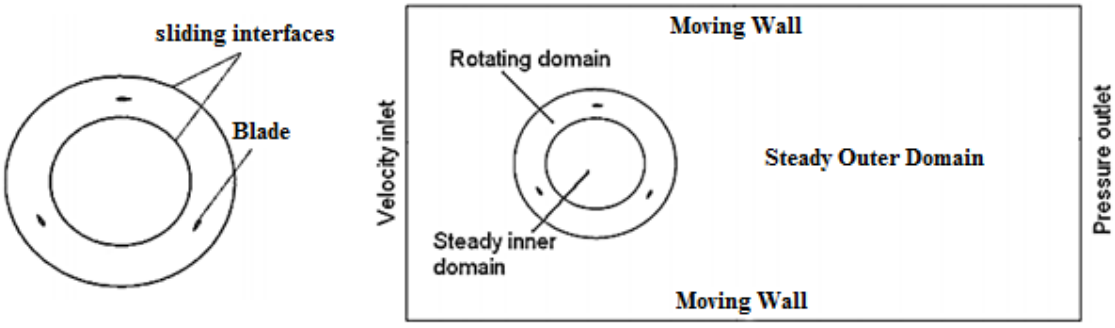

Figure 1.14. Problem domain for sliding mesh simulation of a 3-bladed Darrieus turbine [27]

At the end of a sliding mesh simulation moment coefficients and other performance parameters are readily available for the full 360^{o} range of the azimuth angle. No special treatment is necessary to take wake formation and blade interaction into account. But a separate simulation should be done for each *TSR* value of interest. In

this thesis sliding mesh simulations are done. Dynamic mesh technique is one alternative to sliding mesh, but due to very costly mesh motion and new mesh generation calculations at each time step it is rarely used.

In the literature, Lain and Osorio [27] performed 2D sliding mesh simulations for a marine turbine. They emphasize the importance of the use of a proper boundary layer mesh for accurate simulations. For turbulence modeling they preferred SST $k-\omega$ model. They presented time step and mesh independency results. They compared their results with experiments only for a single TSR value, but the match is not good.

Carrigan et al. [28] used this technique for airfoil shape optimization of VAWTs. They reached an optimized shape of NACA 0015 for VAWT applications. They also pay attention to grid independency and suggested the use hybrid grids instead of the structured ones for VAWT simulations. Their 2D unstructured and structured grids needed 55,000 and 100,000 elements, respectively, to get grid independent solutions. They worked with a single step size and the lack of time step independency is a weakness of their work.

Biadgo et al. [29] considered sliding mesh and DMST models together and concluded that DMST model overestimates the maximum power coefficient compared to the sliding mesh (Fig. 1.15). Their sliding mesh simulations were also 2D. They provide no time step or mesh independency details, which reduces the reliability of their results.

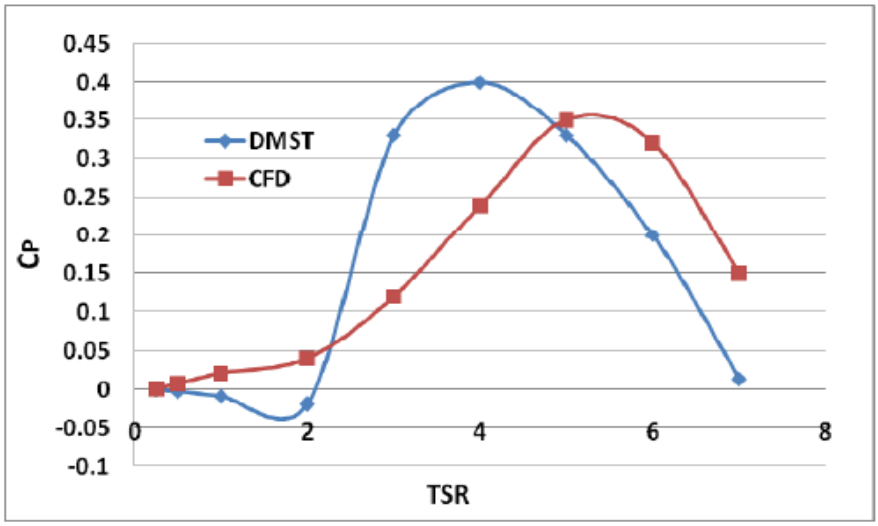

Figure 1.15. Variation of power coefficient with tip speed ratio for DMST and sliding mesh models [29]

Castelli, De Betta and Benini [30] focused on the effect of blade number on the performance of a Darrieus type VAWT. Their 2D study makes use of blades with NACA 0025 airfoil sections. They investigated turbines with three, four and five blades with the same chord length and concluded that the three bladed configuration gives the best turbine output. Absence of any time step or mesh independency details and the lack of boundary layer meshes around the blades are the main weaknesses of this study. Also, there is not any discussion about the effect of blade number for the same solidity ratio. This can cause misleading results because increasing blade number by keeping the chord length constant increases the wake interactions between blades. It is possible to reach different conclusions if the total chord length or solidity ratio is kept constant as the number of blades change.

Howell et al. [31] attempted to compare 2D and 3D simulations of a three bladed Darrieus turbine and supported their study with wind tunnel tests at wind speeds of 5.07 m/s and 5.81 m/s. Comparison of their experimental and numerical results are given in Figs. 1.16 and 1.17. As seen from the figures, 3D simulation results match with the experiments better than 2D results. Similar to other studies insufficient information is given about time step and mesh independency. Also they covered a

narrow *TSR* range. In addition, their 3D simulations did not show the periodicity of torque coefficient.

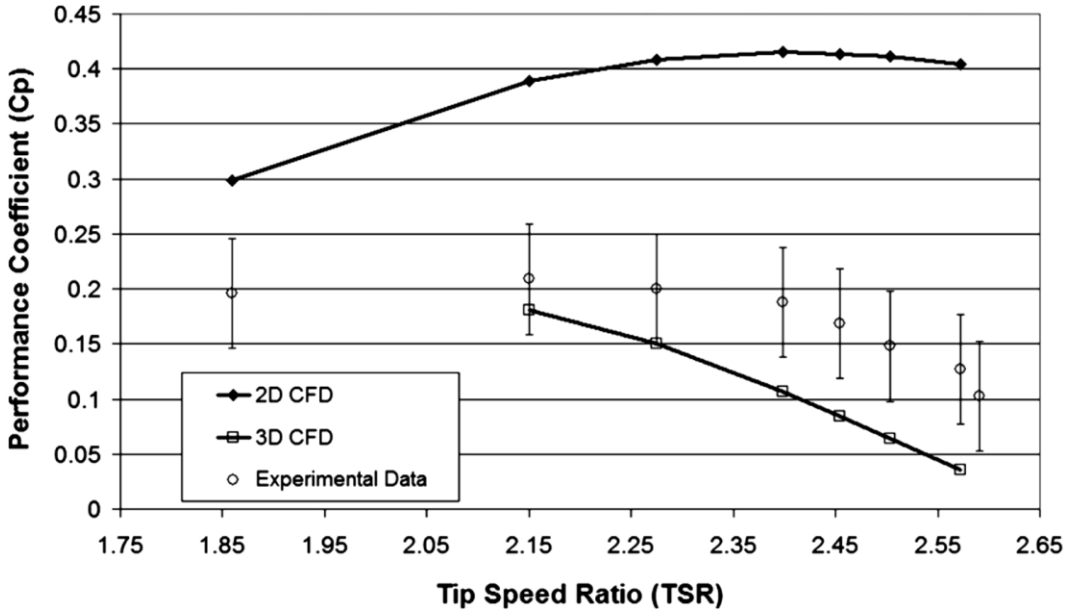

Figure 1.16. Comparison of experimental and numerical results at 5.07 m/s wind speed [27]

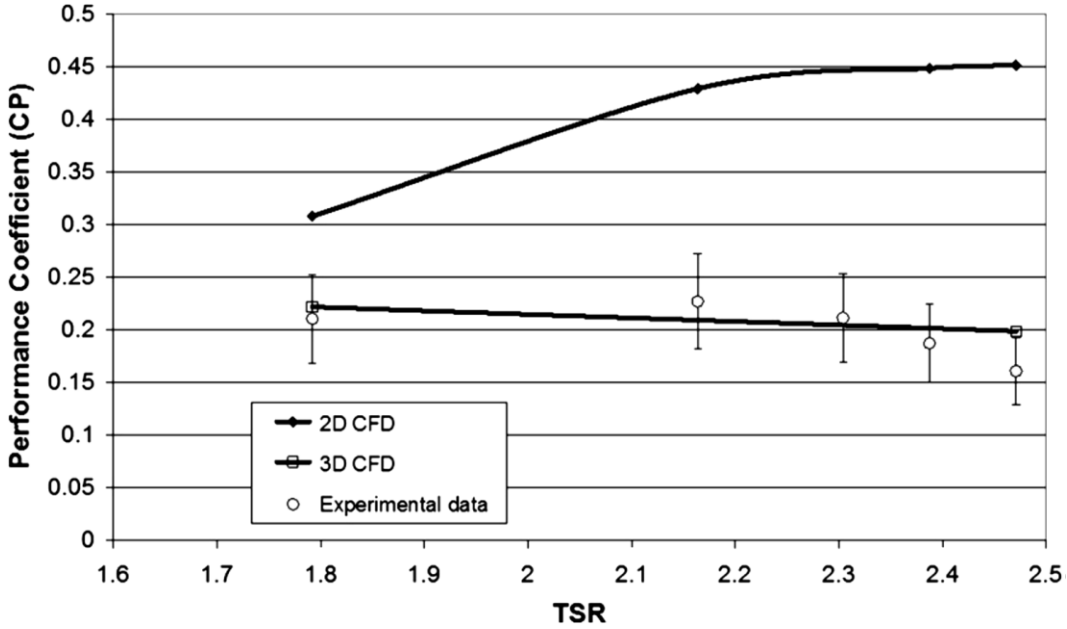

Figure 1.17. Comparison of experimental and numerical results at 5.81 m/s wind speed [27]

1.5. THE CURRENT WORK

In this study performance of Darrieus type VAWTs are predicted using sliding mesh based CFD simulations using ANSYS Fluent software. Straight bladed turbines are considered and simulations are done in 2D using SST $k-\omega$ turbulence model. A broad range of *TSR* values is studied while keeping free stream wind speed, turbine diameter, blade height, blade airfoil and chord length fixed. Two- and three-bladed configurations are studied at fixed solidity ratio by paying special attention to their start up issues. Very special care is put to provide details about the boundary layer and far field mesh generation, grid independency, time step independency and residual tolerance independency studies. In Chapter 2 parameters of the simulated turbine are given. Results of grid, time step and residual tolerance independency tests are provided. In Chapter 3 results of overall and start-up performance simulations of two- and three-bladed turbines are presented. Chapter 4 summarizes the work, lists the conclusions reached and provide suggestions for possible future work.

CHAPTER 2

SELECTION of TURBINE PARAMETERS and GRID, TIME STEP AND RESIDUAL TOLERANCE INDEPENDENCY SIMULATIONS

In this study, the sliding mesh approach is used to predict the performance of Darrieus type turbines numerically. Accuracy and efficiency of the simulations are closely related to the grid and time step used and it is important to make sure that the results are independent of them. Without detailed independency runs, it is not possible to claim any reliability of the results. However it is quite difficult to find studies in literature that pay proper attention to this. Also in many of the studies details of boundary layer and far field meshes are not shared in enough detail so that the simulations can be repeated.

In this chapter first the fixed parameters of the Darrieus turbine that is going to be simulated are selected. Next, the solver settings used in Fluent are shared. Than the details of a series of grids generated for a single blade VAWT are given. With all these selections time step independency, residual tolerance independency and grid independency simulations are performed and results are presented.

2.1. TURBINE PARAMETERS

This thesis study originated from a Teknogirisim Funding project supported by the Turkish Ministry of Science, Industry and Technology. The project included the design and manufacturing of a Darrieus type wind turbine, as well as primitive performance data collection through field tests. The one year project was completed at 20.04.2012. Some of the selections that are mentioned in the coming paragraphs were decided during that project and directly used in this thesis.

Considering the general preferred use VAWTs in small-scale applications it is decided to work with a turbine that will generate 270 W optimum power at the rated wind speed of 10 m/s, which are typical values seen in commercial VAWTs [32]. In addition, 270 W power is selected due to the high level of availability of low power electric generators in the market. However, the simulation free stream wind speed is

fixed at 7 m/s due to its higher energy frequency of occurrence at 10 m, a typical height for small-scale VAWTs. A sample of wind frequency distribution at 10 m height is shown at Figure 2.1.

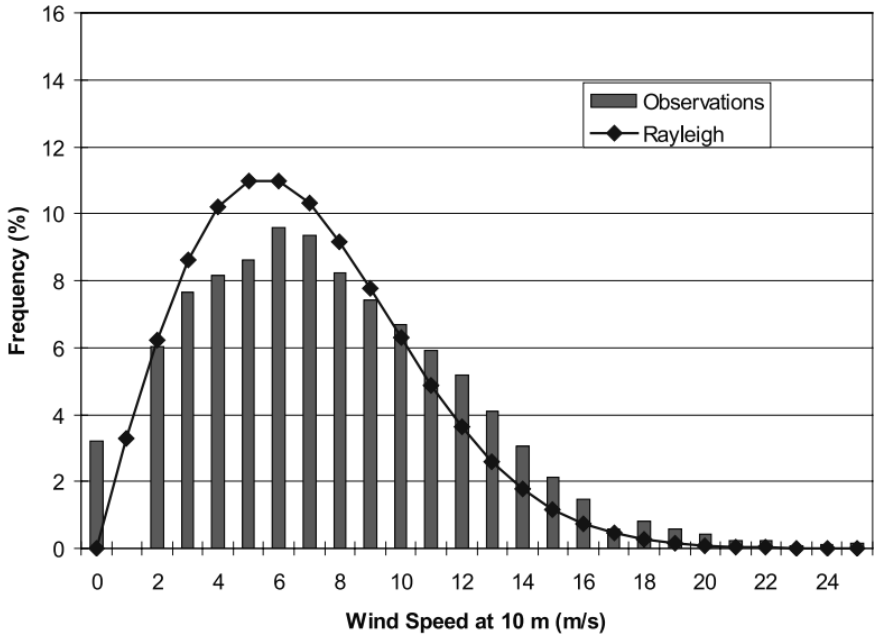

Figure 2.1. Wind speed frequency distribution at 10 m [33]

As given in Eqn. (1.4) power output of a wind turbine scales with the cube of the free stream velocity. Therefore 270 W optimum power at 10 m, reduces to 92.5 W at the selected 7 m/s wind speed. In order to be able to determine the dimensions of the turbine, it is required to fix the power coefficient, for which a value of 0.4 is used. Selections done up to this points are summarized in Table 2.1.

Table 2.1. Selected Free Stream Wind Speed and the Desired Output Parameters

Simulation Wind Speed (V_∞)	7 m/s
Desired Power Output (P)	92.5 W
Desired Power Coefficient (C_P)	0.4

Reference projected area of the turbine can now be calculated using Eqn. (1.9) as follows

$$A = \frac{P}{0.5\,\rho_a C_P V_\infty^3} = \frac{92.5}{0.5\,(1.225)(0.4)(7^3)} = 1.1\ \text{m}^2 \qquad (2.1)$$

Now it is appropriate to determine H/D and c/R ratios. Following the work of Islam [34], values of 0.892 and 0.15, respectively, are considered first. These values are modified slightly so that geometrical parameters that are easier to work with can be obtained. Final selections are given in Table 2.2.

Table 2.2. Selected Geometric Parameters

$\boldsymbol{H/D}$ **= 0.909**	
Diameter (D)	1.1 m
Height (H)	1 m
$\boldsymbol{c/R}$ **= 0.178**	
Radius (R)	0.55 m
Chord Length (c)	98 mm

For the airfoil selection, the study of Graham and Panther [35] is used. By the help of their results on the effect of thickness for NACA series airfoils and Islam's studies [34], NACA-0021 is selected as the blade profile. Also blade number is selected to be 3, which is the most commonly used design, but as will be seen in Chapter 3, simulations are also done for 2-blade configurations.

2.2. COMPUTATIONAL DOMAIN, BOUNDARY CONDITIONS and SOLVER SETTINGS

As mentioned previously, unsteady simulations are performed using the sliding mesh approach. Two-dimensional problem domain used for this purpose is shown in Fig. 2.2. Blades of the turbine are located inside the rotating circular ring zone shown in gray color. This ring, with the blades and the mesh in it, rotates CCW with a constant

angular velocity that is determined by the simulated tip speed ratio, while the inner and outer zones are kept fixed, resulting in a mesh sliding at the zone interfaces. In Fig. 2.2 all dimensions are given in terms of the turbine diameter D, which is 1.1 m. Determination of how far the outer boundaries should be placed required a number of trial runs, details of which are not given here.

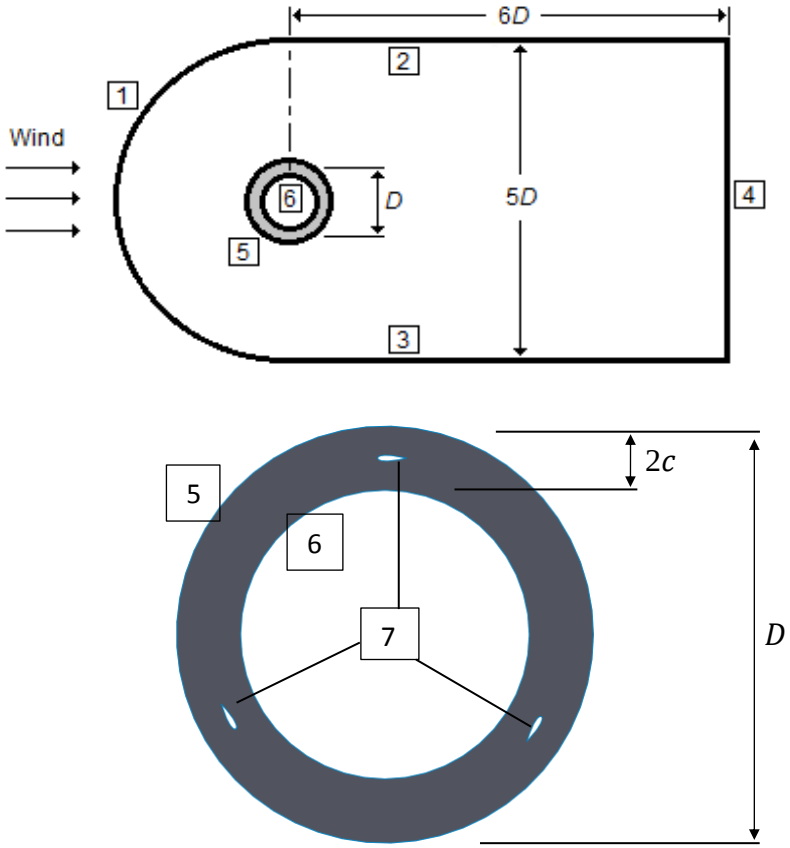

Figure 2.2. Problem domain, boundary labels and the rotating ring zone with 3 blades in it

At the exit boundary, labeled as 4 in Fig. 2.2, constant pressure boundary condition is specified. Constant wind speed is specified on all far field boundaries (1, 2 and 3). On the two circles enclosing the rotating ring zone (5 and 6), interface type boundary condition is specified and no slip boundary condition is used on the rotating blades (7).

To obtain the results of Chapter 3, either two or three blades are used inside the ring zone. But in the independency simulations of this chapter only a single blade is considered to decrease simulation times. All unsteady sliding mesh simulations are performed starting from a previously converged steady run with a non-rotating ring zone. This decreases the time to reach time periodicity considerably. Solver parameters used for the steady initialization runs and final unsteady runs are given in Table 2.3. First order upwind discretizations are used for all variables due to stability issues faced with higher order schemes at critical blade positions with severe flow separation.

Table 2.3 Solver Settings used in Fluent

	Steady Initialization Runs	Unsteady Sliding Mesh Runs
Turbulence Model	SST $k-\omega$	
Modeling of Rotating Cell Zone	Moving Reference Frame	Moving Mesh Frame
Pressure-Velocity Coupling Scheme	Coupled	SIMPLE
Gradient Discretization	Green-Gauss Node Based	
Pressure Discretization	PRESTO	
Momentum Discretization	First Order Upwind	
Turbulent Kinetic Energy (TKE) Discretization	First Order Upwind	
Specific Dissipation Rate (SDR) Discretization	First Order Upwind	

2.3. TIME STEP INDEPENDENCY

Flow over the blades of a VAWT is unsteady and time periodic. A proper time step selection is necessary to ensure that the results are time step independent. This selection depends on how fast the turbine is rotating, i.e. the tip speed ratio (TSR) when the wind speed is fixed. All independency simulations of this chapter are performed only for a single tip speed ratio of 3, due to the expectancy of having optimum turbine operation at this value. This value is also high enough to see complex and challenging to solve flow patterns. Also, as mentioned previously, only

a single blade is used to decrease the simulation time. For the time step independency simulations a mesh configuration similar to the *medium mesh* that will be introduced in the Section 2.5 is used. Convergence tolerance values are set to 10^{-6}. Constant rotational speed of the ring zone is selected as $\omega = 38.2$ 1/s, which corresponds to $TSR = 3$.

As shown in Fig. 2.3 the blade rotates a certain amount during each time step. Simulations are done for four different time steps as shown in Table 2.7. The table also gives the amount of blade rotation and total time steps necessary for one full rotation for each case. In presenting the results, these four cases will be referred using the degree of rotations in one time step, instead of the time steps themselves. Although the simulation with the smallest time step size seems to be taking 8 times more computational time than the one having the largest time step, actually the situation is not that bad. Smaller time step results in a more stable solution, which corresponds to reduced number of iterations required for convergence within each time step. Also, maximum iteration limit of each time step is selected as 150, which is large enough to let the residuals drop down to the selected tolerance value of 10^{-5}.

Variation of moment coefficient with position of the rotating blade for different time steps is given in Figure 2.4. The data is collected after a certain number of rotations required to reach time periodicity. Zero degree corresponds to the instant where the blade is located at the top of the ring zone, directly facing towards the wind, i.e. zero angle of attack.

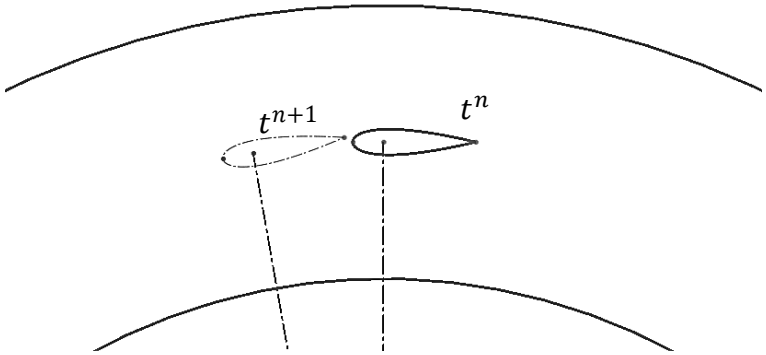

Figure 2.3. Rotation of Blade between Two Discrete Time Levels

Table 2.4. Time Steps used for the Time Step Independency Study

Time step (s)	Blade's rotation at each time step (degree)	Number of time steps necessary for 1 full rotation
0.0004568	1	360
0.0002284	0.5	720
0.0001142	0.25	1440
0.0000571	0.125	2880

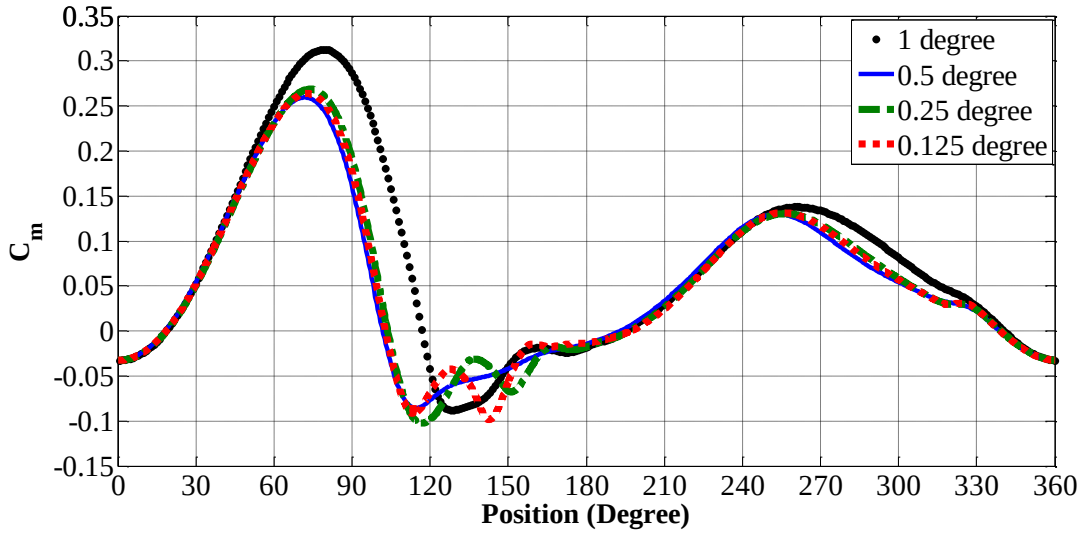

Figure 2.4. Variation of moment coefficient with position of the single blade for different time steps

During the time step independency simulations, the selected maximum number of iterations for each time step turns out to be insufficient to achieve the desired convergence tolerance between the positions of 110^0-160^0 for 1 and 0.5 degree cases. This problem is not observed for the other two cases with smaller time steps. It is observed that less number of iterations are necessary for convergence at each time step as the time step decreases. As seen in Fig 2.4 moment coefficients for 0.125 and 0.25 degree cases are almost identical, except 110^0 - 160^0. In these problematic regions the blade starts receiving the wind from its trailing edge and large separation regions form. But this time duration is small compared to a full cycle. Also moment coefficient values in this part are low, not contributing

significantly to the total power generation. As a result, “0.25 degree case” corresponding to a time step of 0.0001142 s is selected for further simulations.

2.4. CONVERGENCE TOLERANCE INDEPENDENCY

Unsteady pressure based solver of ANSYS Fluent makes use of an iterative solution scheme. At every time step the solution goes through this iterative process during which residuals defined for the continuity and momentum equations as well as turbulence parameters are constantly observed [35]. When the residuals drop below user defined tolerances the iterations are terminated and the calculations of the new time start. By default Fluent uses 10^{-3} for the tolerance of all parameters, which should not be accepted directly, but questioned. Selection of the tolerance values used for the convergence declaration has a significant effect, not only on the accuracy of the results, but also on the solution time.

For the convergence tolerance independency simulations, the time step selected in the previous section is used. The mesh of this section is the same as the previous one. Four different tolerance values are tested and the results are shown in Fig. 2.5 as the moment coefficient versus blade position. The figure shows one full cycle, for which the data is collected after observing periodicity. As seen the results for $5x10^{-5}$ and 10^{-5} are almost identical and it is decided to use the former for further simulations. It is important to note that the default value of 10^{-3} is not appropriate for this problem. It is of course possible to set different tolerance values for declaring the convergence of different parameters, which is not done here. Instead the residuals of all parameters are checked against the same tolerance value.

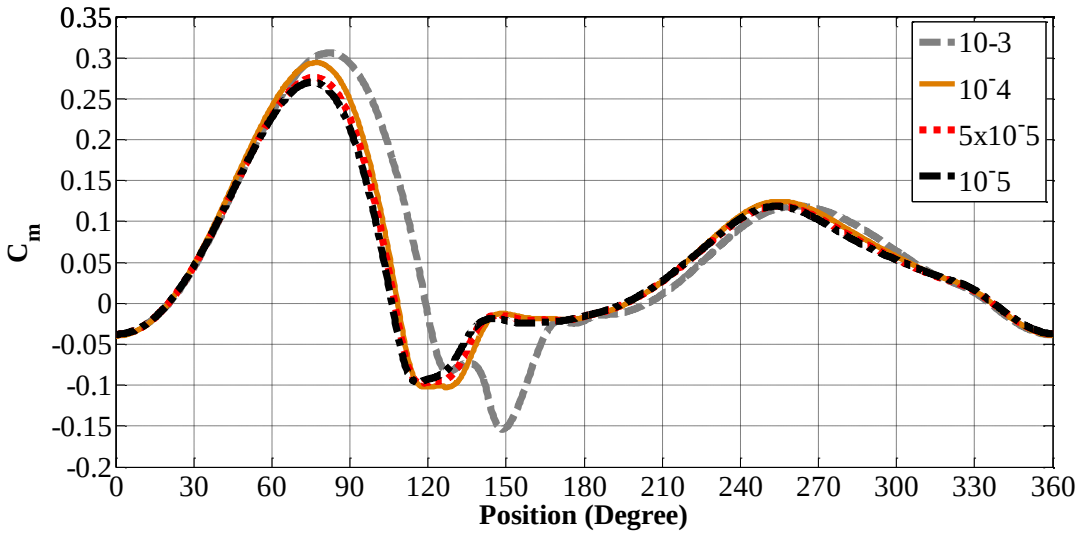

Figure 2.5. Variation of moment coefficient with position of the single blade for different convergence tolerances

2.5. MESH INDEPENDENCY

During the operation of a VAWT, blades are subjected to flow at all possible angle of attacks, sometimes resulting in severe separation. It is impossible to solve the flow field accurately without a carefully generated mesh. In this study, a hybrid mesh, with structured quadrilateral elements inside the boundary layer and triangular elements elsewhere. Three different meshes, labeled as *coarse*, *medium* and *fine* are created. Number of node intervals used along different boundary segments are given in Table 2.5. Boundary labels used in this table are shown in Fig. 2.2. Similar to the previously discussed time step and convergence tolerance independency studies, mesh independency is also done for a single blade.

Table 2.5. Number of intervals used for the discretization of the boundaries for three different meshes

Mesh	1	2 & 3	4	5	6	7
Coarse	50	40	30	225	150	150 x 2
Medium	50	40	30	300	225	250 x 2
Fine	50	40	30	375	300	350 x 2

As presented in Table 2.5, discretizations of the far field boundaries (1, 2, 3 and 4) are kept the same for each mesh. The values used for these boundaries are determined by a set of preliminary analyses. Remaining boundaries (5: outer circle of the ring zone, 6: inner circle of the ring zone, 7: blade) are divided into more and more segments as the mesh is refined from coarse to fine.

Boundary layer meshes created around the blade are controlled as shown in Table 2.6. In simulating a Darrieus turbine it is almost impossible to get acceptable results in an efficient way without using a structured boundary layer mesh. Proper selection of the first layer thickness of the boundary layer mesh is very important to predict the wall shear accurately. In this study, the selection of this value is determined by a series of analyses, in which the value of first layer thickness is decreased to the limiting values that cause convergence problems for the turbulence kinetic energy of the SST $k-\omega$ turbulence model. Table 2.6 shows the smallest allowed values without convergence issues. Triangular elements are used outside the boundary layer, with a smooth transition from fine to coarse towards the far field. Numbers of rows for each boundary layer configuration are selected such that highly skew elements at the interface of structured and unstructured mesh regions are avoided. After obtaining the results it is seen that this actually was a safe-side choice, because boundary mesh regions turned out to be larger than actual boundary layers.

Table 2.6. Boundary layer parameters of each mesh. *c* is the chord length of the blade

Mesh	First layer thickness	Number of rows
Coarse	0.001 *c*	20
Medium	0.0002 *c*	40
Fine	0.0001 *c*	55

With these control parameters, total number of nodes in the *coarse*, *medium* and *fine* meshes turn out to be 35,000, 141,000 and 218,000, respectively. Part of the created meshes around the airfoil can be seen in Fig. 2.6 to 2.10.

Mesh concentration around the blade can clearly be seen in Fig 2.6. Details of the boundary layer mesh are shown in Fig. 2.8. As seen in the figure, thickness of the structured boundary layer mesh decreases as the mesh density around the blade increases. Mesh details around the leading and trailing edges of the airfoil are given in Fig 2.9 and 2.10. For the *coarse* mesh, elements with large skewness are observed due to the long element edges that cannot be fitted properly to the curved leading edge or the sharp trailing edge.

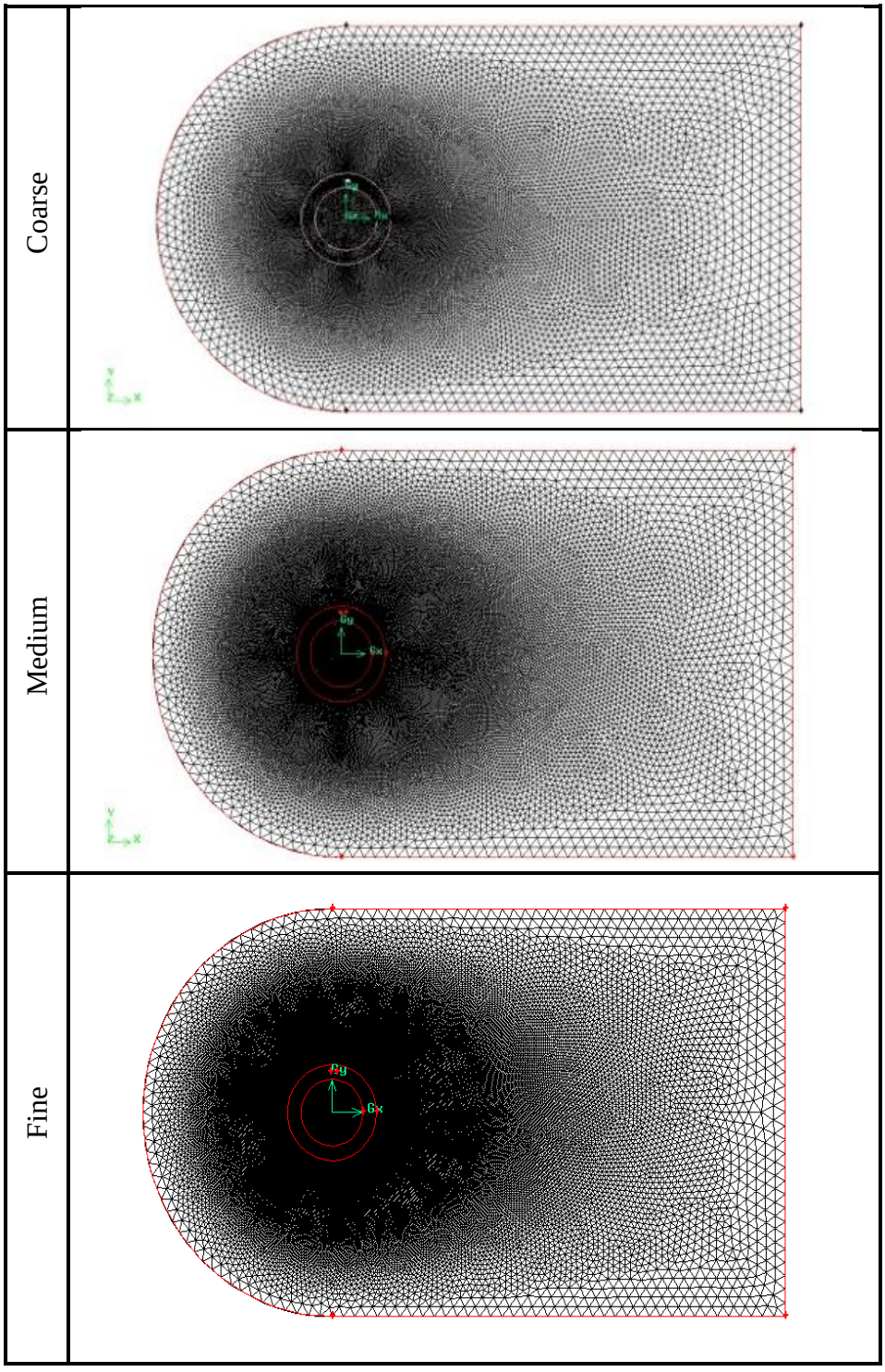

Figure 2.6. Meshes of the problem domain

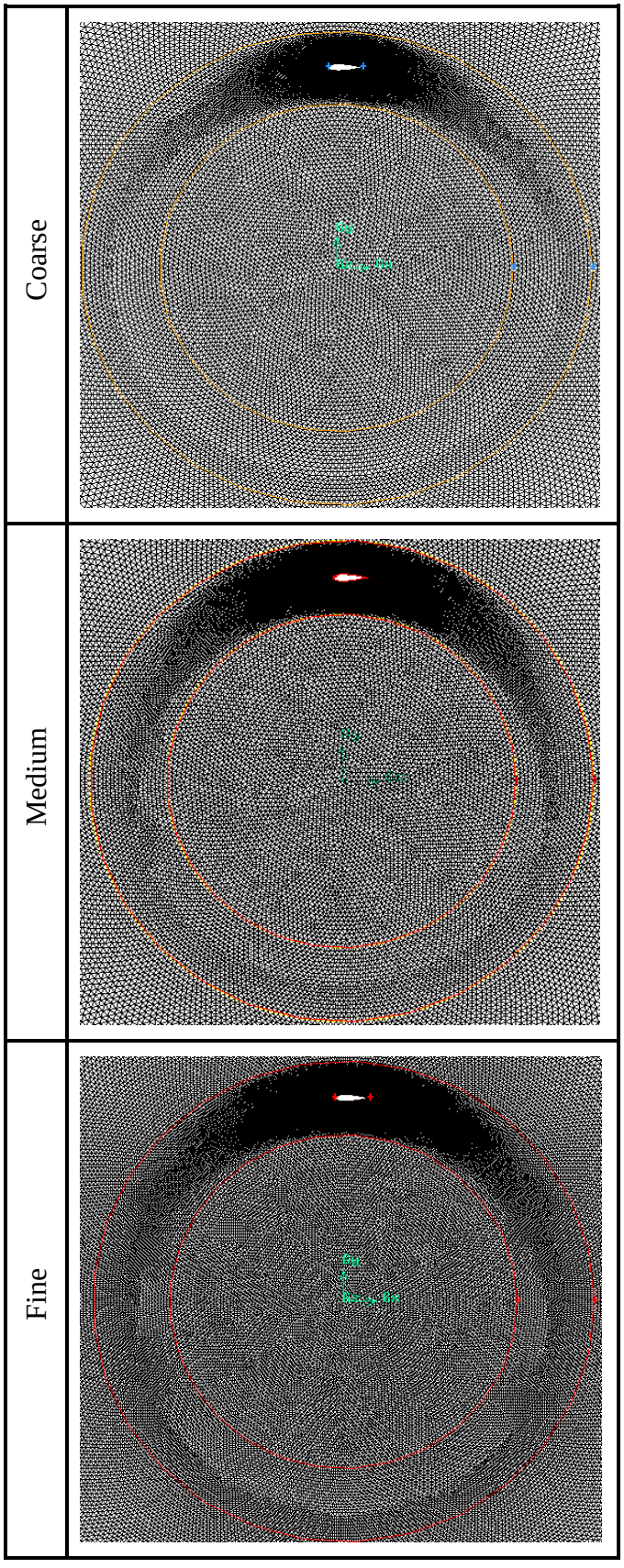

Figure 2.7. Meshes of the rotating cell zone

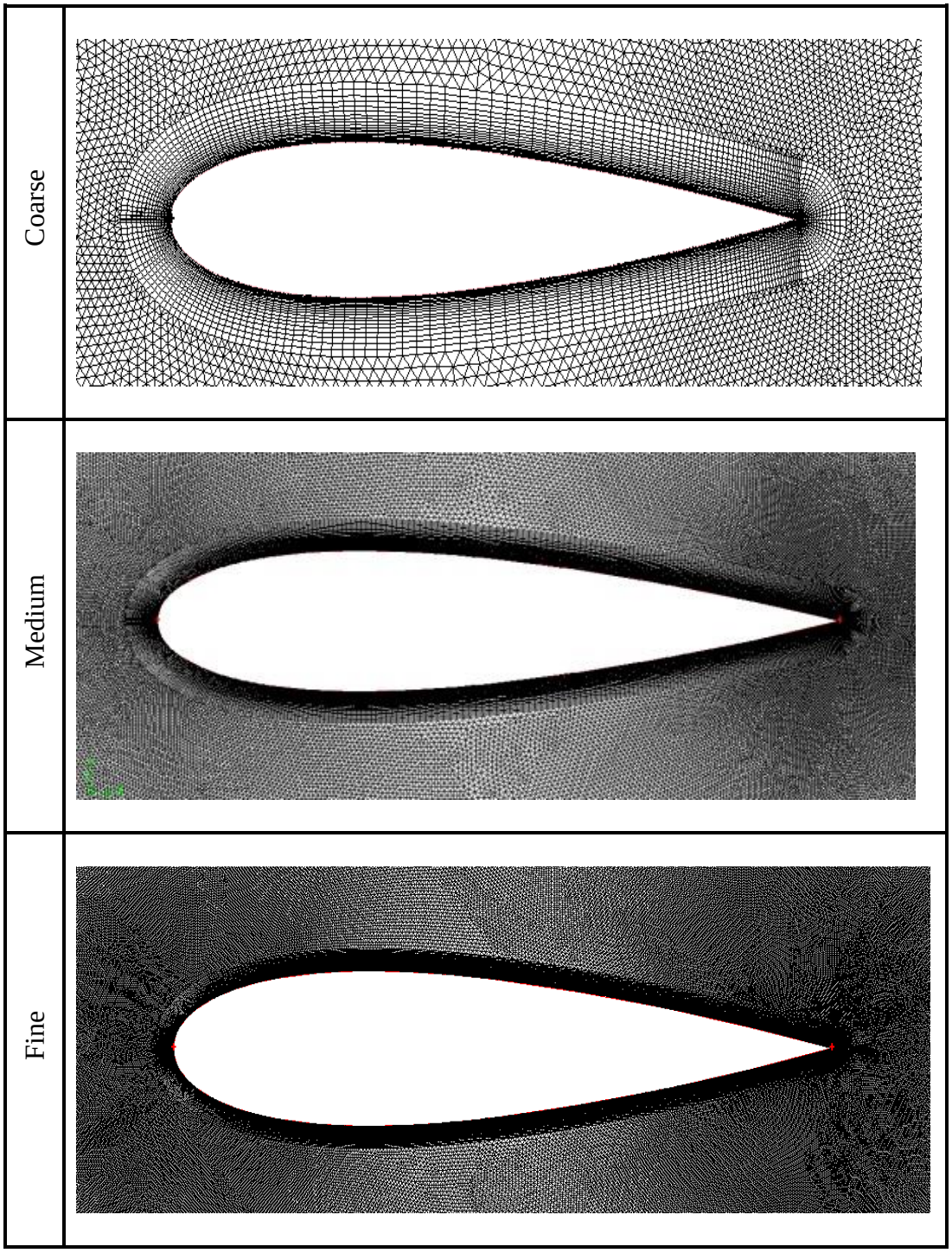

Figure 2.8. Meshes around the blade

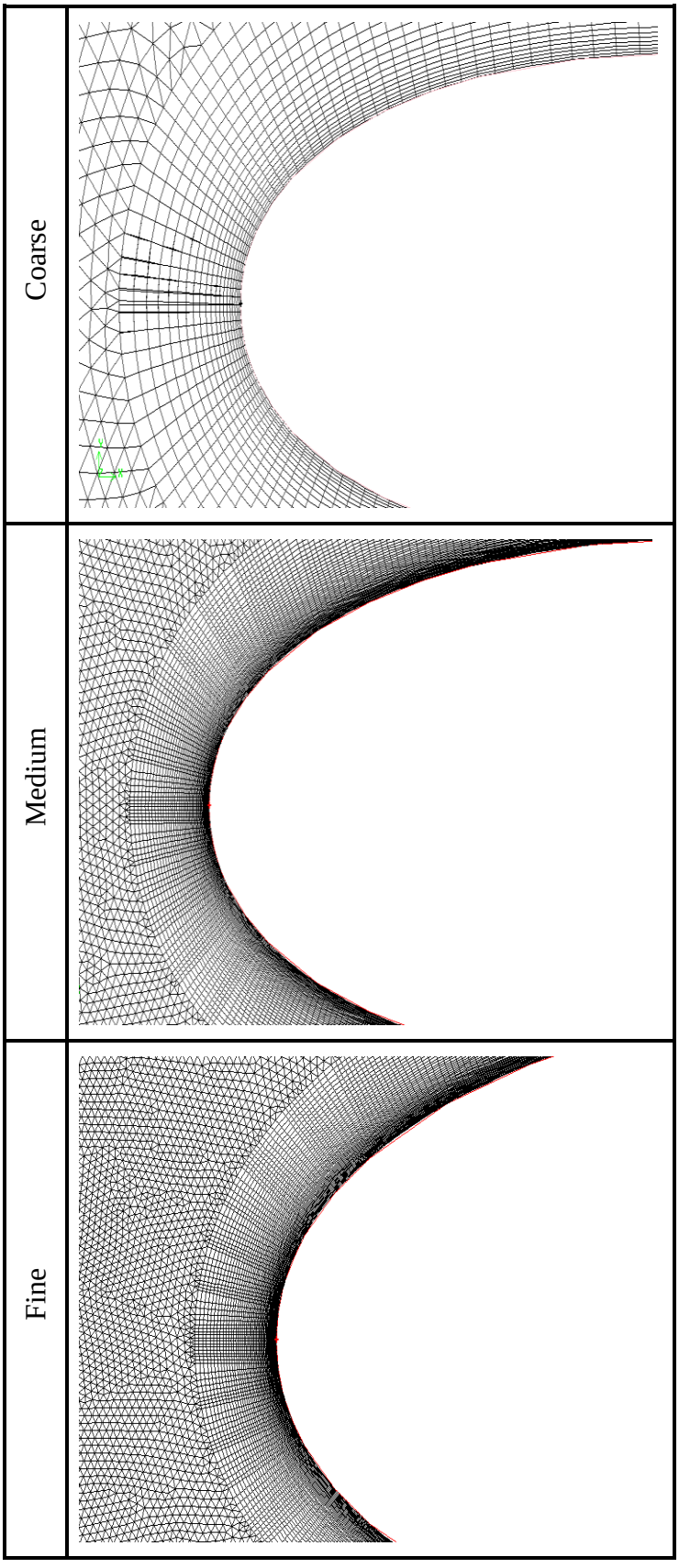

Figure 2.9. Meshes around the leading edge of the blade

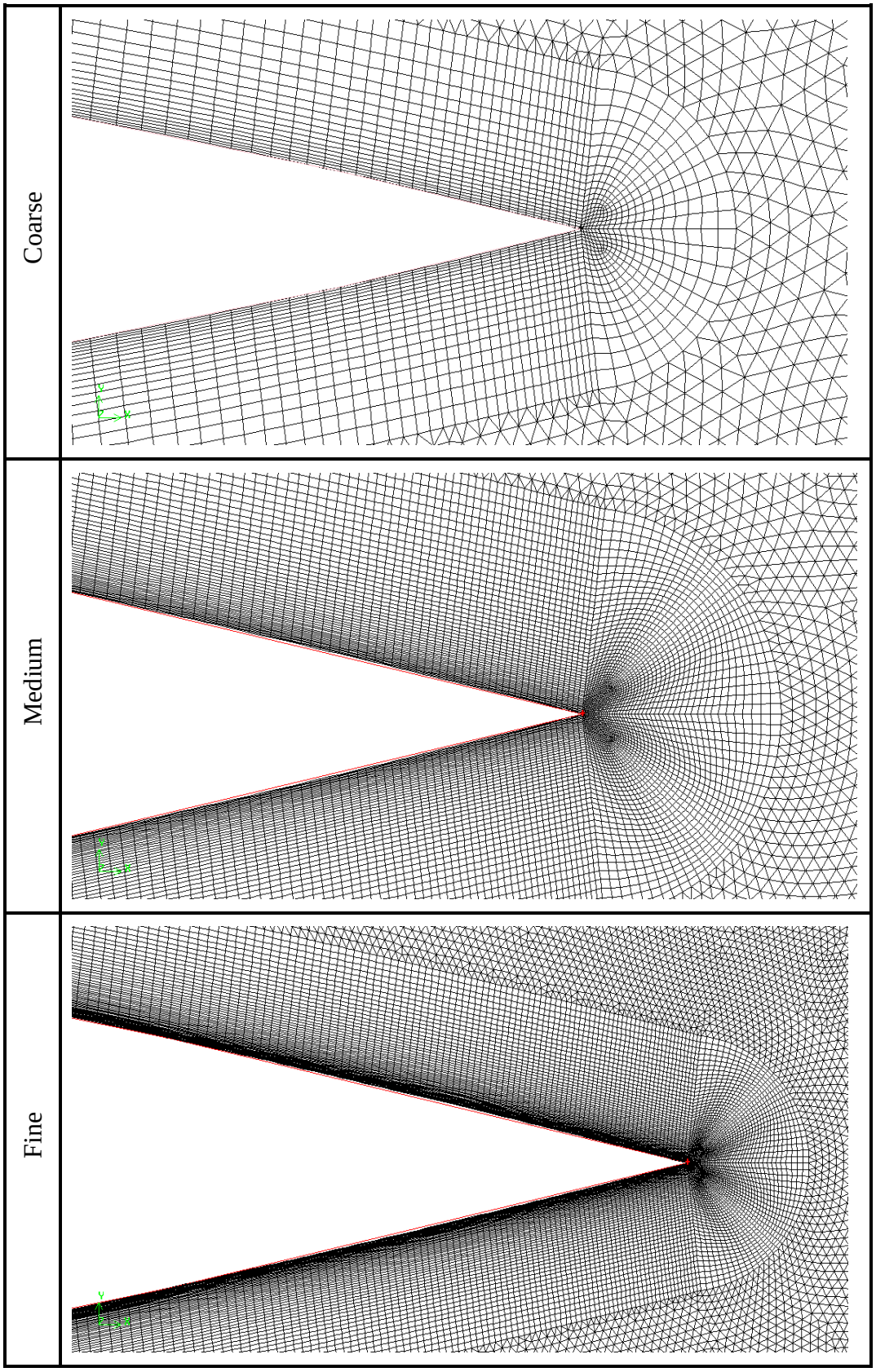

Figure 2.10. Meshes around the trailing edge of the blade

Moment coefficients obtained using different meshes are compared in Fig. 2.11.Time step and convergence tolerance values that were determined in the previous sections are used. As seen in the figure, results of the *medium* and *fine* meshes are very close to each other, while that of the *coarse* mesh do not match with these two. The region of 120° - 150° again poses some challenges, however the problem is not that significant as discussed previously. The results can be used to conclude that *medium* mesh results are good enough and this mesh will be used for the simulations of Chapter 2.

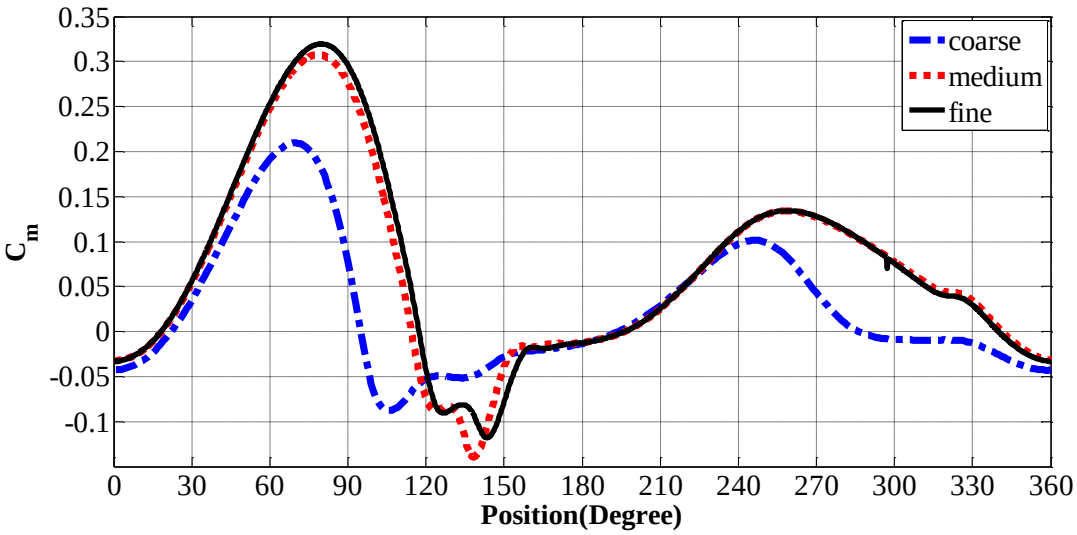

Figure 2.11. Variation of moment coefficient with position of the single blade for different meshes

2.6. VERIFICATION OF THE CURRENT APPROACH

Although careful simulations were done to select the time step, convergence tolerance and mesh, one still needs to compare the results of the current simulations with other sources. One of the most important simplifications used in this study is modeling the turbine as 2D. The obvious reason behind this is the lack of computational resources for unsteady 3D simulations. The appropriateness of SST $k-\omega$ turbulence model can also be questioned, although that selection is already based on the frequent use of this model in the literature for similar applications. However, it is not easy to find reliable computational and experimental Darrieus turbine studies in the literature.

Unlike horizontal axis wind turbines, it is difficult to find real field measurement data for VAWTs in the literature. Very limited number of experimental studies are all performed in laboratory conditions, mostly by rotating the turbine with an electric motor. One valuable study that is unfortunately noticed towards the end of the current thesis work is done by Castelli et al. [36]. They performed both 2D and 3D simulations as well as experimental measurements. Many of their parameters are similar to the ones used in this study, such as the basic dimensions of the turbine, blade airfoil profile and the solidity ratio. But current results can not directly be compared with theirs mainly due to non-matching wind speeds. They worked with a speed of 9 m/s, whereas in the current study wind blows at 7 m/s. To make more reliable comparisons extra simulations for 9 m/s are done at 4 different *TSR* values. In Fig. 2.12 power coefficient vs. *TSR* result of the current three-blade simulations is compared with their numerical and experimental results. Here it is important to note that their 3D simulations were not actually 3D, in the sense that they did not consider the full blades with tip effects, rather only modeled a short portion of them. Their study covered a *TSR* interval of 1.4 - 3.3.

First observation is that Castelli's results do not show a good match in themselves. Their 2D results greatly overestimates the experimental data. Their 3D results on the other hand provides a closer maximum C_P value, however it misses the general trend of the C_P variation and provides unacceptable estimates for low *TSR*s. The current

results for 7 m/s wind speed and the current simulation model adapted for Castelli's configuration for 9 m/s wind speed capture the general trend nicely with a shift towards higher *TSR* values. Low *TSR* estimates match nicely with the experimental data. Compared to experiments, overestimate of maximum C_P can be attributed to the missing struts, blade tip losses and turbine shaft, among all other differences of the two studies.

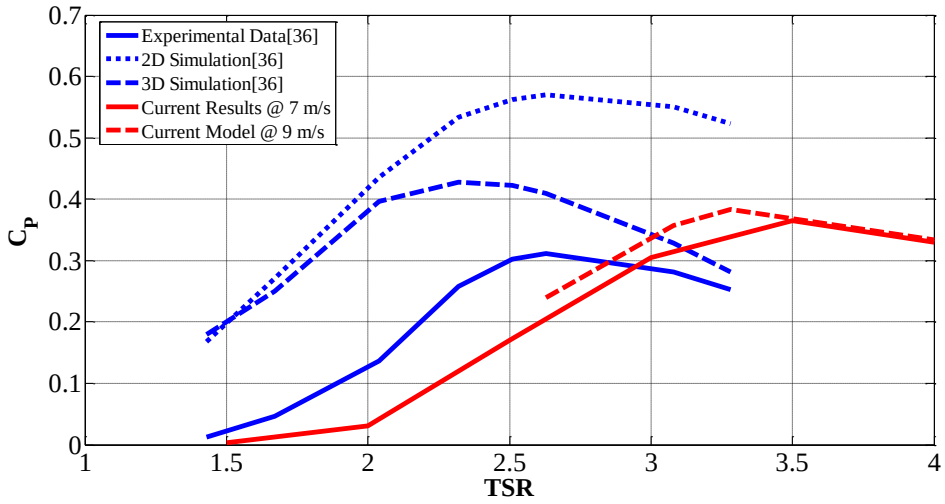

Figure 2.12. Rough comparison of current results (V_∞ = 7 m/s) and current model (V_∞ = 9 m/s) with those of Castelli et al. (V_∞ = 9 m/s) [36]

CHAPTER 3

PERFORMANCE SIMULATIONS

In this part of the thesis, results of the performance simulations will be shared. Turbines with two and three blades will be simulated for 11 different TSR values in the range 0.15 – 4. For a fair comparison of two and three blade configurations, solidity ratio is kept fixed by changing the chord lengths. First, variations of the moment coefficient during a full cycle are discussed for each *TSR*. Critical instants of rotation are analyzed by using pressure contours. Next, the variations of overall performance parameters, obtained by integrating previous results over a cycle, with *TSR* are examined. Details of start-up, transition and optimum operation regions are considered separately. Finally, transient responses of the two- and three-bladed VAWTs from the start-up to optimum operation conditions are obtained.

3.1. SUMMARY OF THE SIMULATION MODELS

Important turbine parameters and solver settings are summarized in Table 3.1. Blade chord length of the three-blade turbine is 98 mm, as used in Chapter 2, but to keep the solidity ratio fixed, chord length is increased to 147 mm for the two-blade case. Outcomes of the independency simulations of are used with proper modifications. Those simulations were done for a single blade and for *TSR*=3 only. But now there are multiple blades and simulations are done for 11 different *TSR* values. These *TSR*s, corresponding rotational speeds and time steps used to simulate them are listed in Table 3.2. As seen, *TSR* values are denser in the lower range to capture the start-up details better. Maximum *TSR* value used is 4 because it is expected to have the optimum point at a lower *TSR*.

Time steps of Table 3.2 use Chapter 2 findings as follows; In Chapter 2, *TSR*=3 case was simulated and the proper time step was decided to be 0.0001142, corresponding to 1440 time steps to complete one cycle. This value of 1440 time steps per cycle is kept fixed to calculate the time steps for other *TSR*s. In other words, time step for each *TSR* is determined through the following formula

$$\Delta t = \frac{2\pi}{1440\ \omega} \tag{3.1}$$

In Table 3.1 it is stated that medium mesh is used for the simulations of this chapter. However, since now there are multiple blades the meshes used are not exactly the ones shown in Chapter 2. But the parameters of Table 2.5 and 2.6 corresponding to *medium* mesh are used so it is safe to call these new mesh as *medium* level meshes too. Actual node counts of the meshes generated for two- and three-bladed turbines studied in this chapter are given in Table 3.3. As seen especially for the three-bladed case, majority of the nodes are located inside the critical ring zone.

Table 3.1. Summary of Performance Simulation Model

Performance	Rated Wind Speed (V_∞)	7 m/s	
	Desired Power Output (P)	92.5 W	
	Desired Power Coefficient (C_p)	0.4 W	
Turbine Geometry	Turbine Diameter (D)	1.1 m	
	Blade Height (H)	1 m	
	Solidity Ratio (Nc/R)	0.534	
	Chord Length (c)	2 blade	3 blade
		147 mm	98 mm
Solver	Turbulence Model	SST $k-\omega$	
	Type of Cell Zone	Moving Mesh	
	Pressure Velocity Coupling	SIMPLE	
	Gradient Discretization	Green-Gauss Node Based	
	Pressure Discretization	PRESTO	
	Momentum, Turbulent Kinetic Energy and Specific Dissipation Rate Discretization	First Order Upwind	
Other Parameters	Time Step Size	$2\pi/(1440\omega)$	
	Number of Time Steps for 1 Cycle	1440	
	Convergence Residual	$5\text{x}10^{-5}$	
	Mesh Configuration	Medium	

Table 3.2. Rotational Speeds and Time Steps Used for Each *TSR*

TSR	ω [1/s]	Δt [s]
0.15	1.909	0.0022865
0.30	3.818	0.0011432
0.50	6.364	0.0006859
0.70	8.909	0.0004900
1.00	12.727	0.0003430
1.50	19.091	0.0002286
2.00	25.455	0.0001715
2.50	31.818	0.0001372
3.00	38.182	0.0001142
3.50	44.545	0.0000980
4.00	50.909	0.0000857

Table 3.3 Node Counts of Meshes used for Two- and Three-Bladed Turbines

Number of Blades	Total Node Count	Nodes in the Ring Zone
2	85,000	59,000
3	292,000	263,000

3.2. PERFORMANCE RESULTS FOR DIFFERENT *TSR*s

Variations of moment coefficients with the blade position for a full cycle of two- and three-bladed turbines are given in Fig. 3.1, 3.4, 3.5 and 3.6. In these figures 0^o corresponds to the instant when one of the blades is placed at the top of the ring zone (See Fig 2.2).

Figures 3.1a and 3.1b are for the smallest three *TSR* values for two- and three-bladed turbines, respectively. First observation is that each C_m plot shows a repeating pattern. For the two-bladed turbine, there is a phase difference of 180^o between the blades and the plots of Fig. 3.1a repeat themselves two times in a full cycle. For the three-bladed turbine (Fig. 3.1b) there are 3 repetitions. Therefore it is enough to concentrate on only one of these repeating parts.

The second observation is that the graphs are very oscillatory around their respective mean values. In Fig. 3.1a, the two-bladed turbine provides 26, 14 and 8 local peaks for *TSR* = 0.15, 0.3 and 0.5, respectively. At these low rotational speeds the turbine is in its start-up phase and these instantaneous C_m plots can be taken as a warning for considerable mechanical vibrations during the operation of the turbine. Vibrations are expected to be more severe for the two-bladed one due to very sudden oscillations of C_m between maximum and minimum peak values. As *TSR* increases number of the oscillations drop and the turbine starts to operate more smoothly. For the smallest *TSR* value of 0.15 the turbine is rotating at 1.9 rad/s, which creates a linear speed of $\omega R = 1$ m/s at the blade. Compared to the wind speed of 7 m/s, this value is too small to create a significant directionality or time-periodicity to the operation of the turbine and flow field around the blades is dominated by the blowing wind. This clearly demonstrates the well-known start-up problem of VAWTs.

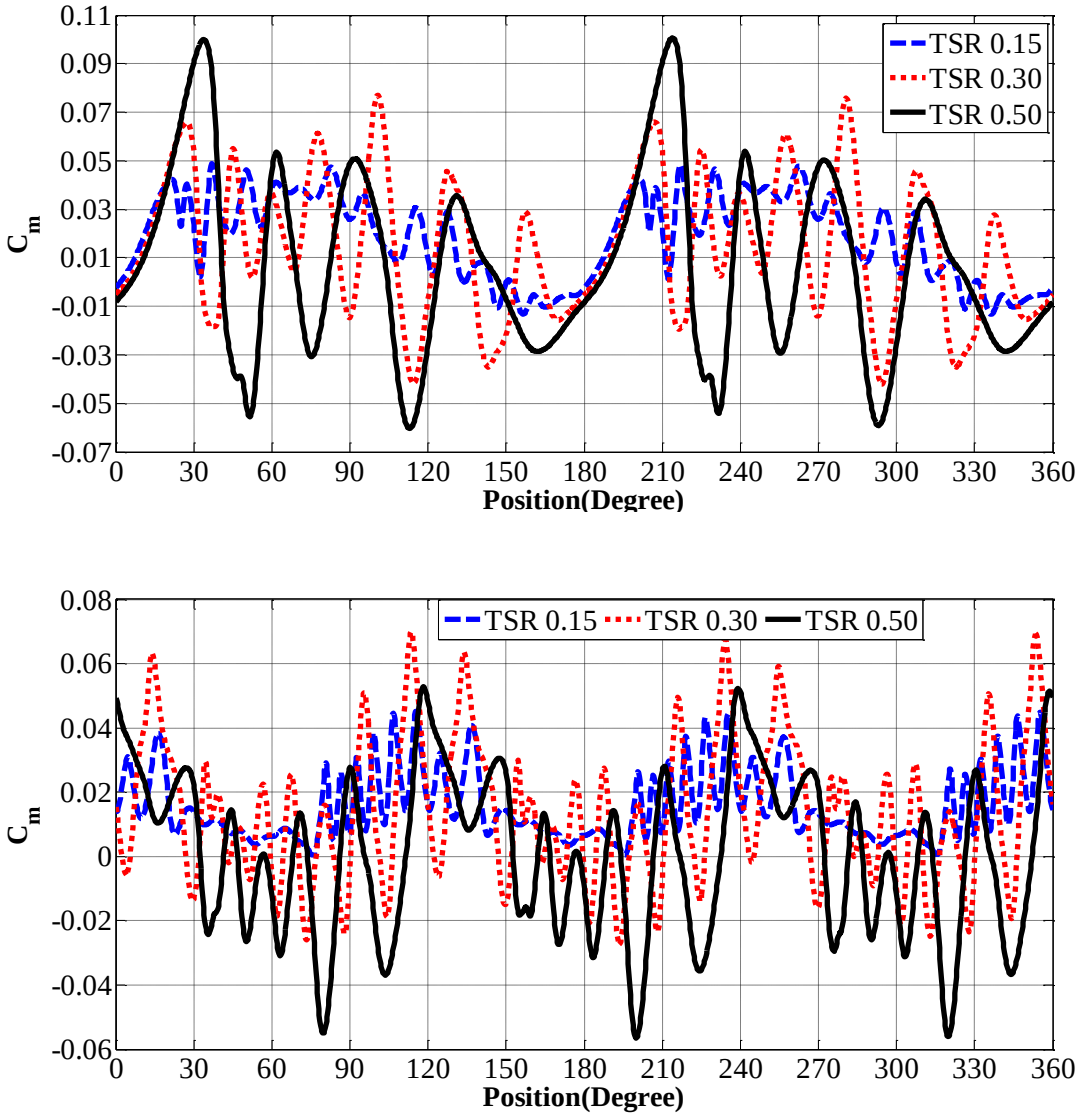

Figure 3.1. Variation of moment coefficient with the blade position at *TSR* 0.15, 0.30 and 0.50 for **a)** two-bladed VAWT (top) and **b)** three-bladed VAWT (bottom)

If the turbine rotates by itself without any wind blowing over it, it is expected to see a pure swirling flow around it. But when the wind blows over the blades it creates regions with significant pressure and velocity changes. Location and magnitude of these changes greatly affect the lift and drag forces and the turbine performance. Fig. 3.2 and 3.3 show velocity and pressure contours over one of the blades of the two-bladed turbine at 120^{o} position.

Figure 3.4 shows the variation of C_m with position for *TSR* values of 0.75, 1.0 and 1.5. Compared to the lower *TSR* values of Fig. 3.1, these plots are less oscillatory as the turbine leaves its start-up phase. Especially for *TSR* =1.5 the upward shift towards positive values is clearly seen, indicating a more expected operation of the turbine.

TSR = 1.5 means that the blade's linear velocity due to its rotation is $1.5V_\infty$= 10.5 m/s. At this *TSR* value the turbine is rotating at 19.1 rad/s, which seems to be enough to suppress aimless fluctuations seen in Fig. 3.1.

In Fig. 3.5 we see that as *TSR* continues to increase, the upward shift of C_m curves also continue for the three-bladed turbine, suggesting that it is headed to its optimum operating points. However, for the two-bladed one C_m drops after *TSR* = 2.5, suggesting that the optimum operating point of the two-bladed turbine is around this *TSR* value. At *TSR* = 3, with only 2 maximum and 2 minimum peaks, the C_m curve of the two-bladed turbine is almost harmonic. Similar can also be said for the three-bladed turbine.

Figure 3.6 shows the momentum coefficient curves for the largest two *TSR* values that are tested. The plots are harmonic and free of extra oscillations. When considered together with Fig. 3.5, C_m curve of the two-bladed turbine is in a clear drop between *TSR* 2.5 and 4.0, suggesting that it already passed over its optimum operating point at around *TSR* 2.5. A similar, but not that sharp drop is also seen for the three-blade turbine and it reaches its optimum operation point around *TSR* = 3.5. Therefore the two-bladed turbine reached its optimum operating point at a lower *TSR* value than the three-bladed one. This observation will be clarified in the next section.

TSR = 0.15	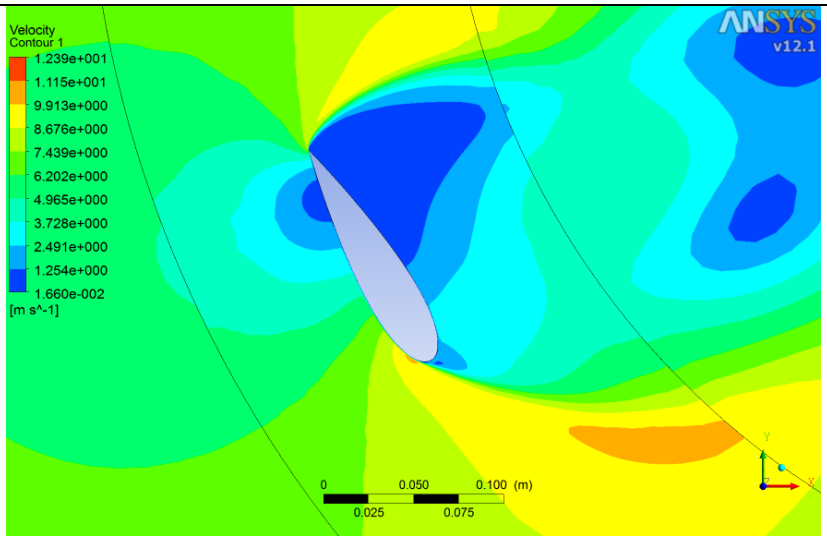
TSR = 0.30	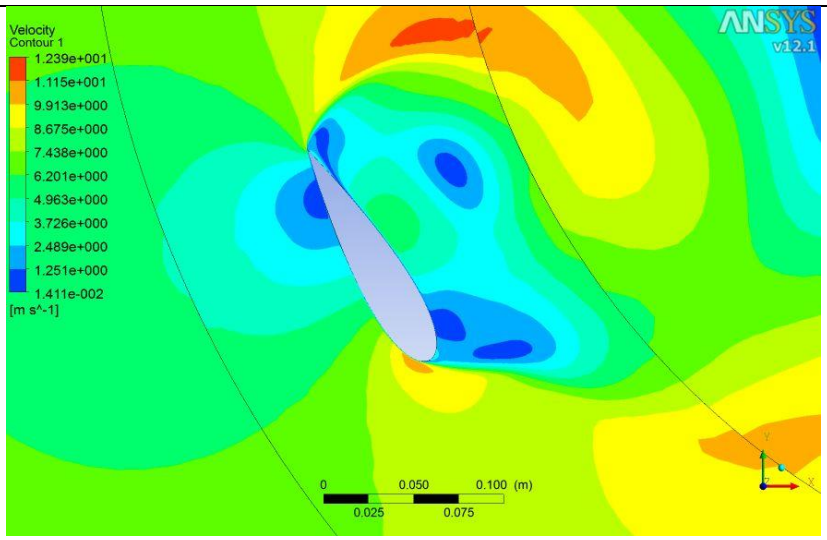
TSR = 0.50	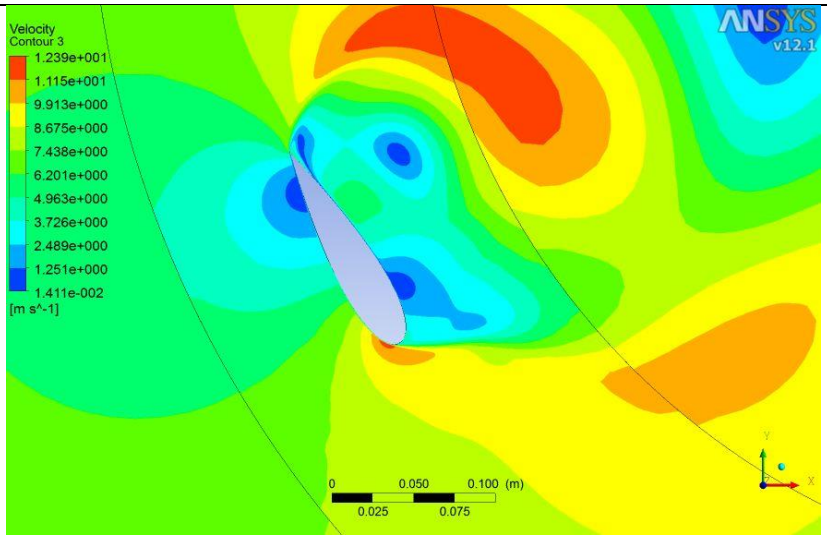

Figures 3.2. Velocity field around the blade at the position of 120° for two-bladed VAWT

TSR = 0.15	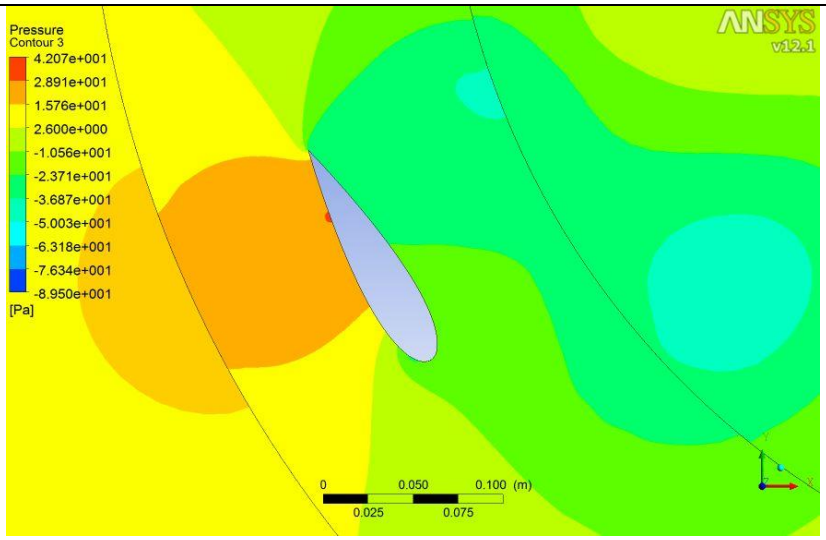
TSR = 0.30	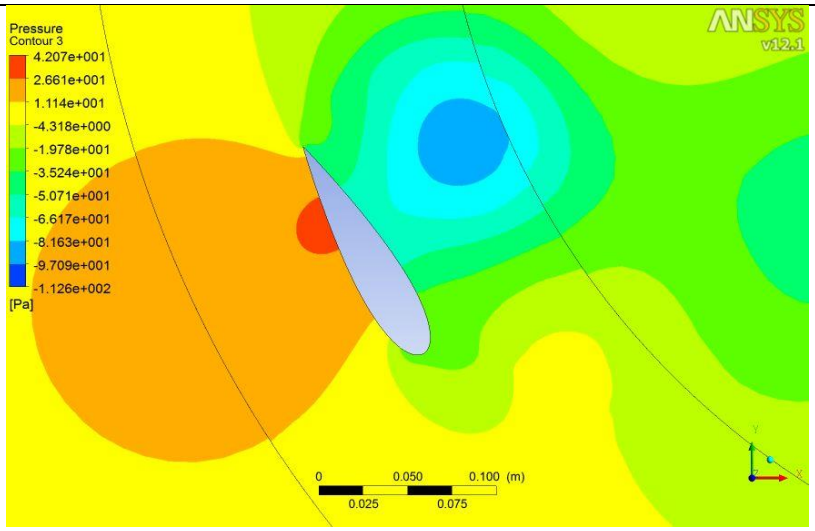
TSR = 0.50	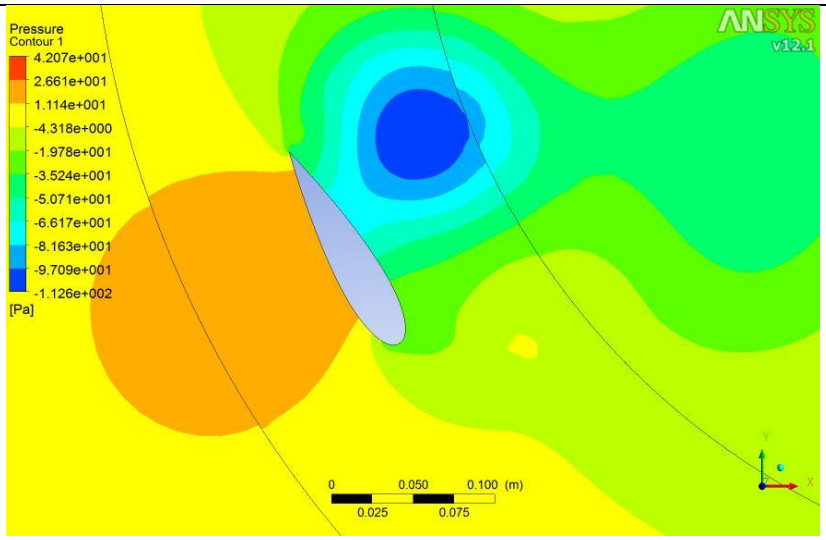

Figure 3.3. Pressure field around the blade at the position of 120° for two-bladed VAWT

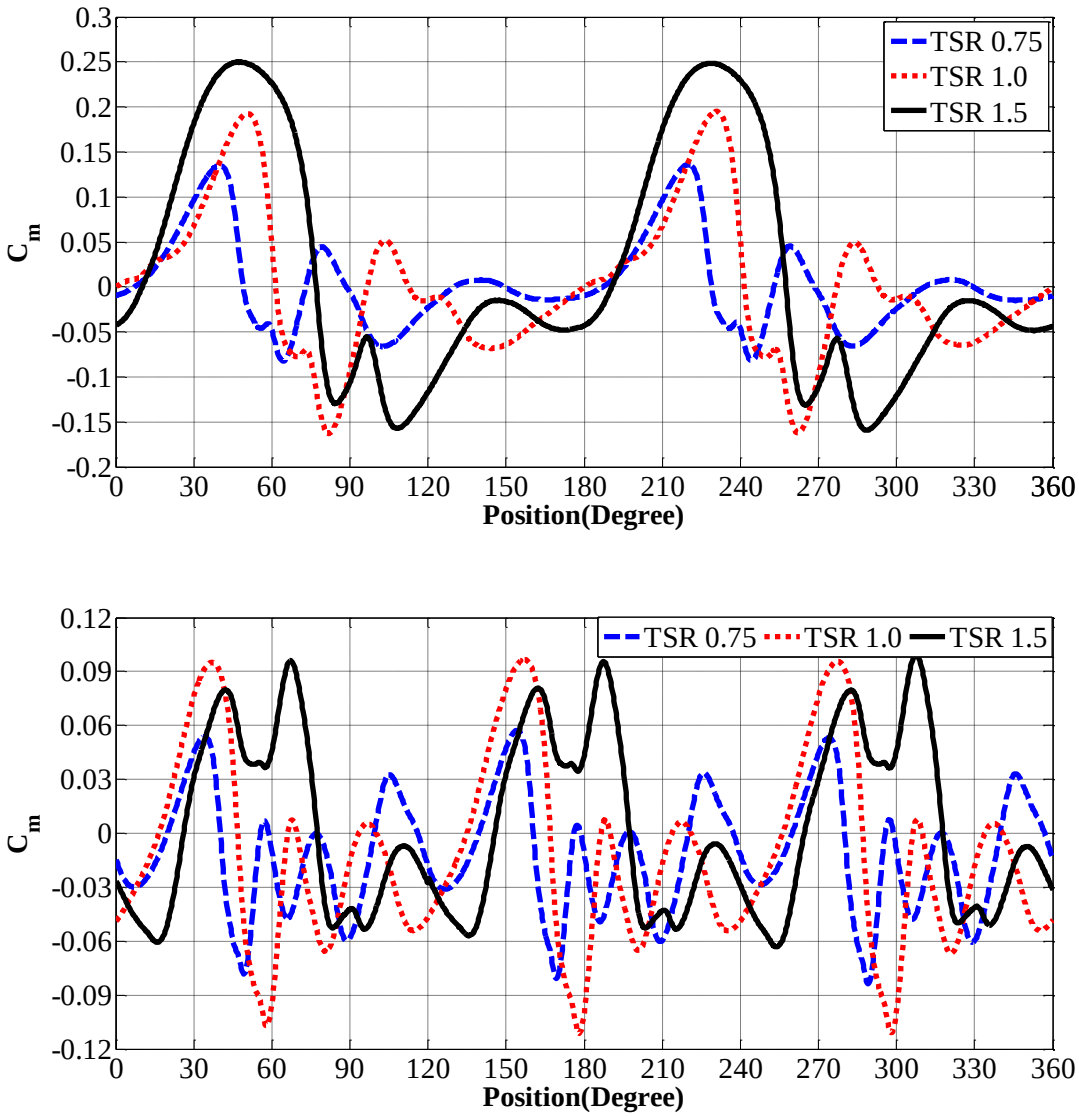

Figure 3.4. Variation of moment coefficient with the blade position at *TSR* 0.75, 1.0 and 1.5 for **a)** two-bladed VAWT (top) and **b)** three-bladed VAWT (bottom)

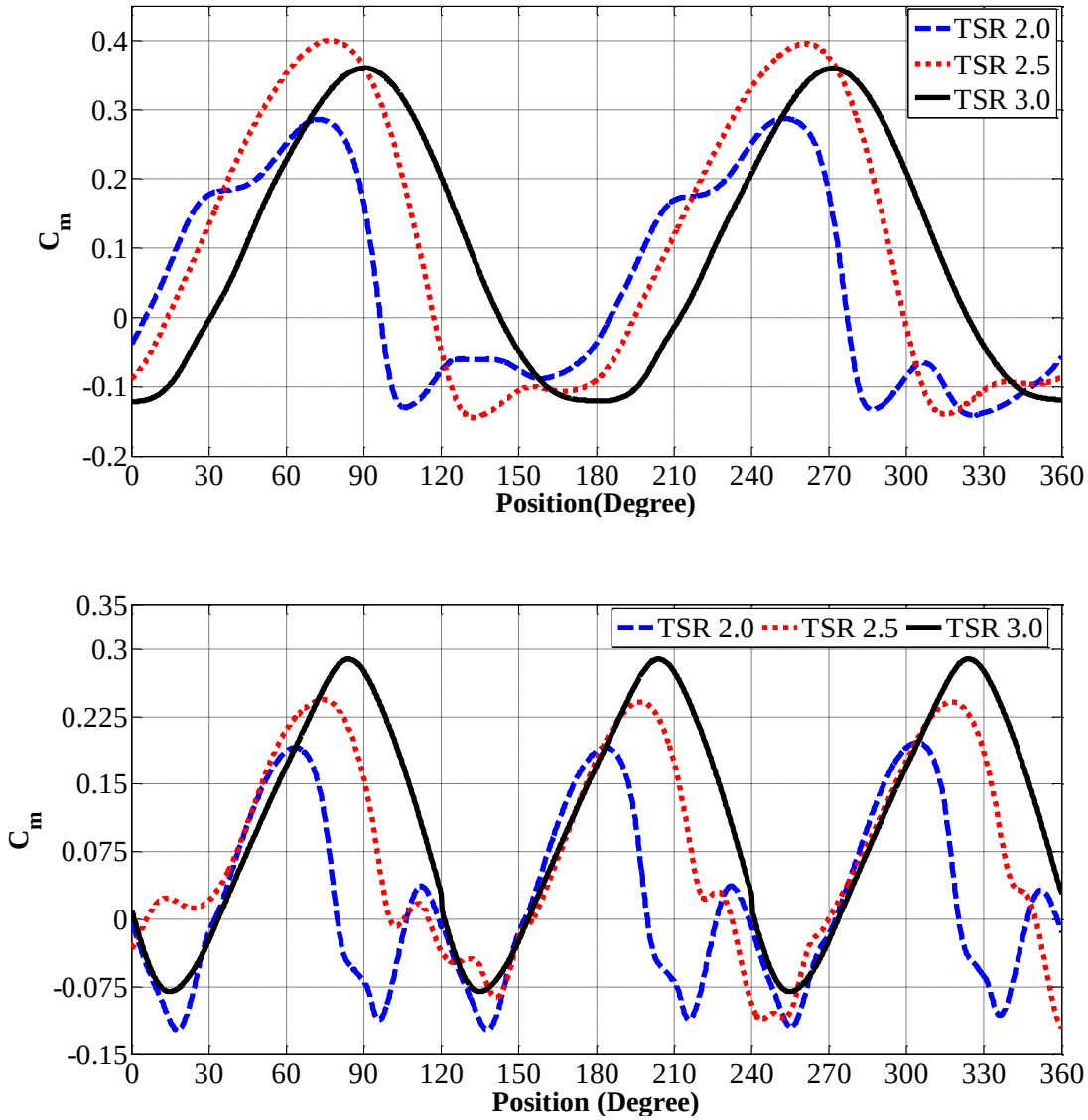

Figure 3.5. Variation of moment coefficient with the blade position at *TSR* 2.0, 2.5 and 3.0 for **a)** two-bladed VAWT (top) and **b)** three-bladed VAWT (bottom)

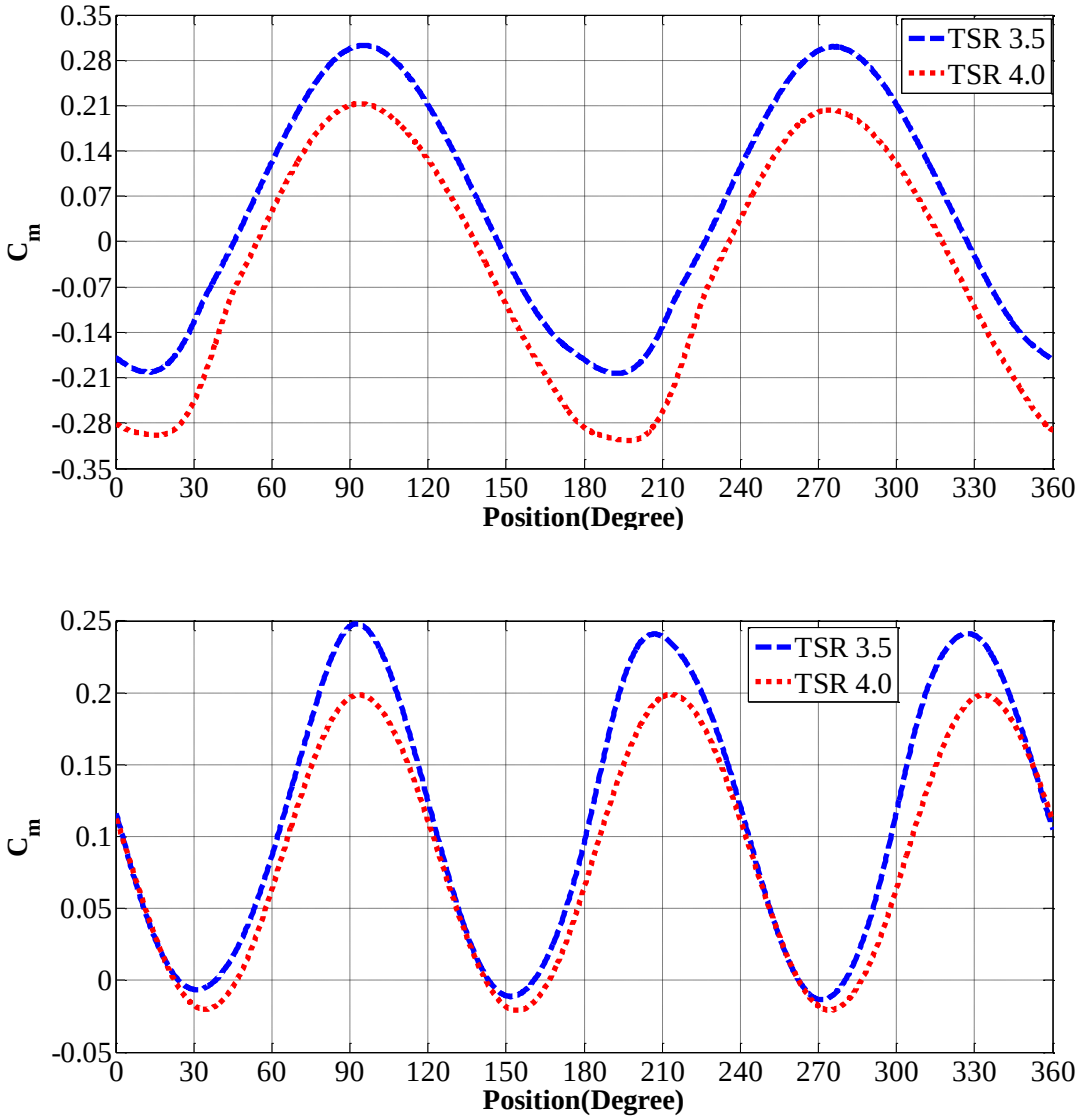

Figure 3.6. Variation of moment coefficient with the blade position at *TSR* 3.5 and 4.0 for **a)** two-bladed VAWT (top) and **b)** three-bladed VAWT (bottom)

As the optimum operating points of the turbines are roughly detected it is time to share more velocity and pressure contours obtained at *TSR* values close to them. In App. A and B velocity and pressure contours around one of the blades of the two-bladed turbine are given at intervals of 30^o for *TSR* = 3. The most efficient operation position, as also seen in Fig 3.5a is 90° in which both blades are perpendicular to the wind. The lest efficient operation position is 180° for which one blade is at the top and the other is at the bottom. The locations and value of negative and positive

pressure regions on the blades have significant effect on the turbine performance. The highest positive pressure values on the leading edge of the top blade are obtained at the least efficient turbine position and generate drag force on that blade and the turbine. In contrast, the highest negative pressure value on the same leading edge location is observed at the most efficient turbine position. It generates thrust effect on that blade and moment on the turbine. It is noted that the positive moment output of the turbine is almost totally dependent upon the blade at the upwind region.

3.3. OVERALL TURBINE OUTPUTS

Figure 3.7 shows the variation of the overall moment coefficient with *TSR*. Overall C_m's are obtained by integrating the time dependent C_m's of previous section over a one full cycle of turbine's operation. Curves of Fig. 3.7 are based on 11 different *TSR* simulations. Three different regions are circled in Fig. 3.7. These regions, also shown in Table 3.4, correspond to the start-up, transition and optimum operation conditions of the turbine. At the start-up both turbines seem to provide a similar overall C_m trend. However, three-bladed one is advantageous in this region due to its more stable behavior in terms of vibratory behavior that is discussed in the previous section. More about this will also be said in the next section. The passage from start-up to transition is sharper for the three-bladed turbine and after *TSR* = 0.5 it gives negative moment coefficients. To prevent or pass the transition region quickly a control system should be used in actual field applications. This vibratory behavior is one of the most important disadvantages of symmetric airfoils such as the one used in this study. After *TSR* = 1 both turbines show an increasing overall C_m behavior with increasing TSR. Two-bladed one reaches its optimum point at around *TSR* = 2.5, which happens at 3.5 for the three-bladed one. After the optimum points, higher rotational speeds cause a drop in the C_m curves.

Fig. 3.8 compares C_m variations of two- and three-bladed turbines and also provides the corresponding moment values, which are calculated using Eqn. (1.8). In Fig. 3.9 generated power and power coefficients of the two turbines are compared. Power and power coefficient values are obtained using Eqn. (1.10) and (1.11).

Using Eqn. (1.4) and (1.7) it is possible to obtain the available power as

$$P_{avail} = \frac{1}{2}(1.225)(1.1)(7)^3 = 231 \text{ W} \quad (3.1)$$

In Fig. 3.9 maximum generated power values are read as 54.7 W and 84.5 W, for two- and three-bladed turbines, respectively. Comparing these values against the available power of 231 W, turbine efficiencies turn out to be 23.8 % and 36.5 % for two and three blades, respectively. Remember that at the beginning of Chapter 2, in Table 2.1, the desired power output was set as 92.5 W. This output was taken from Islam's study [14], which used three blades with a modified NACA 0021 airfoil to achieve it. Power output of the current three-bladed simulations is close to the desired one. However, two-bladed turbine cannot supply it. This is the main reason why three-bladed Darrieus turbines are preferred over two-bladed ones.

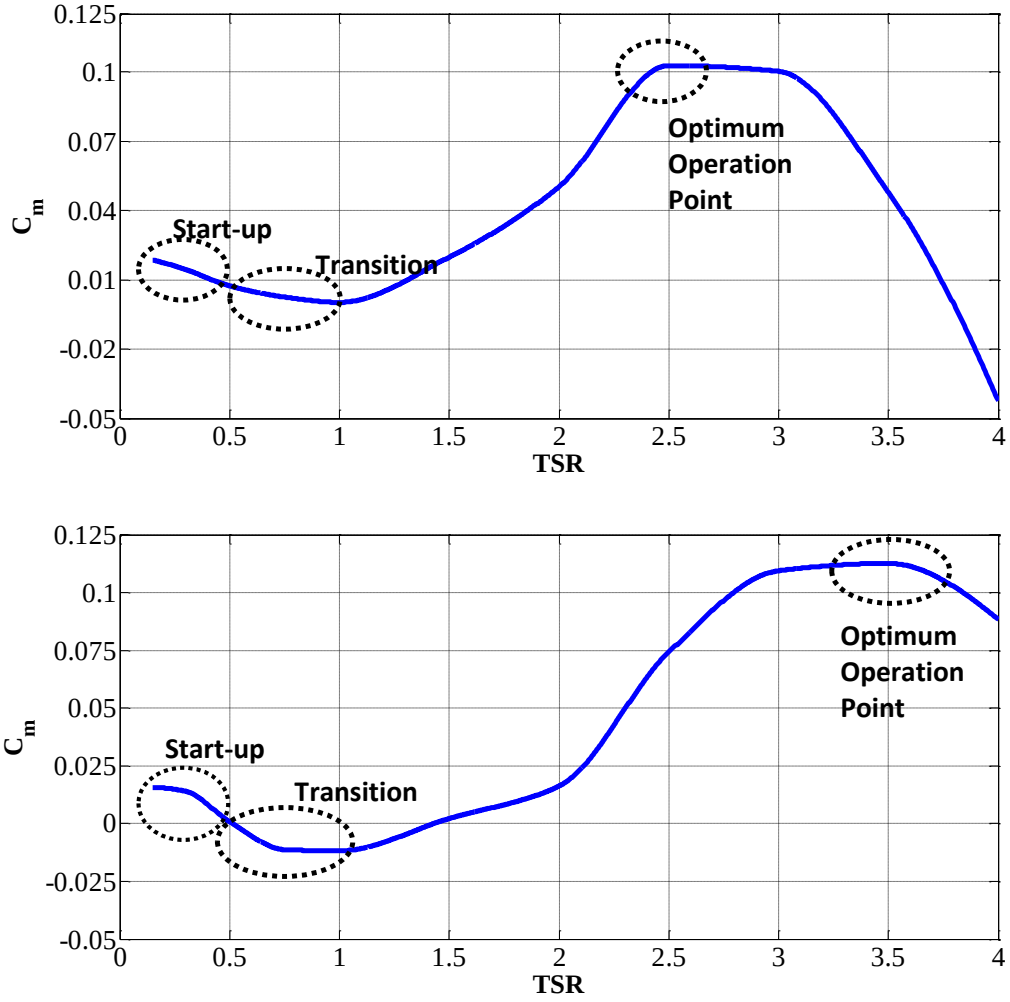

Figure 3.7. Variation of overall moment coefficient with *TSR* for **a)** two-bladed and **b)** three-bladed VAWTs

Table 3.4. Critical TSR Ranges used to Evaluate the Performances of VAWTs

Turbine	Start-up Range	Transition Range	Optimum Operation Range
2-bladed VAWT	*TSR* : 0 - 0.5	*TSR* : 0.5 - 1.0	*TSR* : 2.5
3-bladed VAWT			*TSR* : 3.5

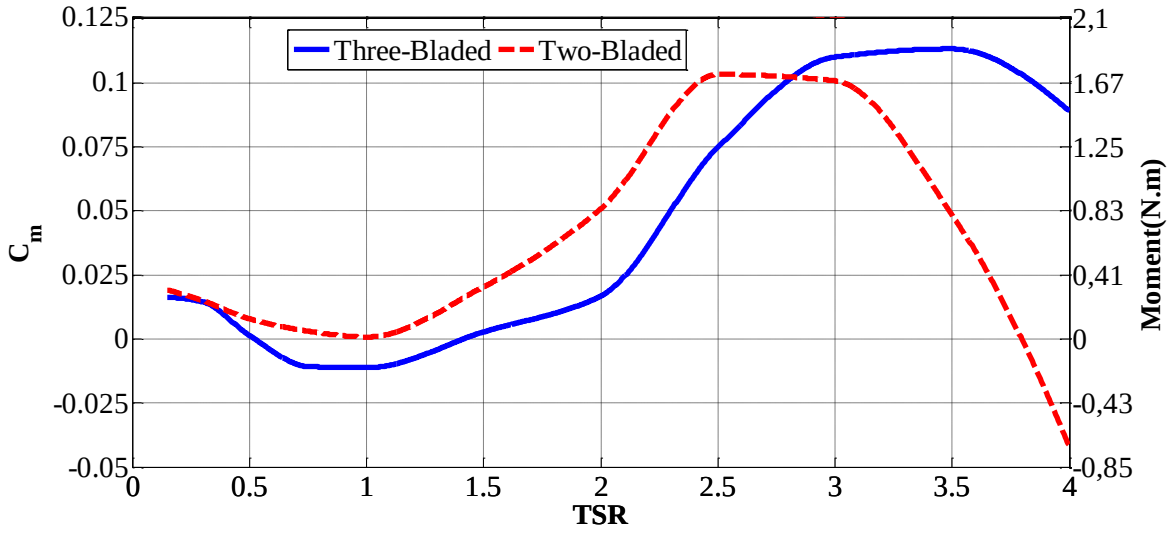

Figure 3.8. Variation of overall moment coefficient and moment with *TSR*

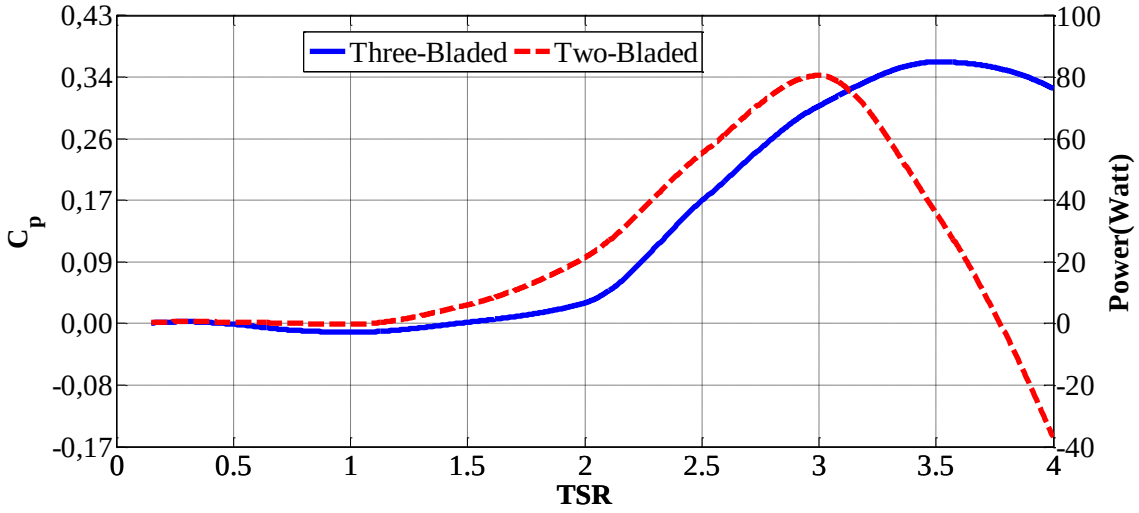

Figure 3.9. Variation of overall power coefficient and power generated with *TSR*

It can be concluded that, to maximize the power output, two- and three-bladed turbines should operate at speeds corresponding to *TSR* = 2.5 and 3.5, respectively. These are the steady design speeds of the turbines. It is also important to mention that these peak points should also be selected as the design points of the corresponding electric generator systems. Although the overall power coefficient of the two-bladed turbine at *TSR* = 3.0 is higher than the one at *TSR* = 2.5, its optimum operation point is determined at the second one since its maximum torque generation is obtained at that point and the electric generator systems need more torque to increase their rotational speed. Then, it is the optimum operation and design point of the turbine with electric generator application.

Moment or moment coefficient curves are widely used to compare performances of different turbines. But such a comparison can cause misleading results. For example, in Fig. 3.8 two-bladed turbine shows higher values of overall moment at the start-up and transition ranges. But the three-bladed one is preferable due to lower vibrations it causes in these ranges. Therefore it is advised that the overall moment curves should only be used to determine the optimum operating region and to calculate the overall power coefficients.

3.4. TIME DEPENDENT RESPONSE OF THE VAWTS

Straight bladed Darrieus type VAWTs are known to have start-up issues. That's why these turbines are usually supported by extra starter mechanisms and batteries. To improve this behavior it is important to understand what actually happens during the start-up and transition regions. From a numerical point of view this requires FSI simulations which will take the turbine from its initial non-rotating state and speed it up to its steady rotation. However such a simulation is quite challenging and none is found in the literature. To put a bit of understanding to the time dependent speeding of a Darrieus turbine, a different and simple approach is used. In this approach, data of the simulated 11 *TSR* values are used to let the turbine rotate by each of them for a certain amount of time before shifting to the next. As the number of simulated *TSR* values increase this approach may provide more realistic results.

Results of this study are presented in Fig. 3.10. One needs to be careful about these figures, which are generated by proper combination of C_m vs. position figures of Section 3.2. In these figures time axes do not correspond to the actual time, in the sense that in real life the turbines' time dependent behavior will not be exactly like this, i.e. they will not rotate at a certain *TSR* for a specified time before switching to the next. Rather they will constantly change their rotational speeds before reaching to their optimal values. Fig. 3.10 is generated by assuming that the turbines start their motion at t = 0 with *TSR* = 0.15, the smallest simulated *TSR* value. They turn with this *TSR* for 1 cycle before switching to *TSR* = 0.3 at t = 3.3 s. They turn with this new *TSR* another cycle and at about t = 5 s they switch to *TSR* = 0.5 with which they go through additional two rotations. These three cycles with the defined TSR values takes almost 6 seconds, which as mentioned previously is not meant to be a realistic estimation.

C_m curves of Fig. 3.10 are further analyzed in Figs. 3.11 - 3.13. Fig. 3.11 gives the RMS, mean and standard deviation values of different TSRs used in Fig. 3.10. Fig. 3.12 is generated to better see the peak-to-peak moment coefficient changes of each TSR. Finally Fig.3.13 is the fast Fourier transform (FFT) of Fig. 3.10. It is useful to see the dominant frequencies in the vibratory operation phases of the turbine, which might be helpful in the structural design and material selection.

Although being rather crude, Fig. 3.10a gives a perspective of what these turbines might go through during their start-up. In the first 3.3 seconds, moment coefficients are all positive for the three-bladed turbine, but there are negative values for the two-bladed one. Although the mean C_m value of the latter is higher than the one of the former at whole start-up region, its standard deviation and RMS values are always higher (see Fig. 3.11a). It decreases the stability of rotations and increases the fatigue load on the turbine blades. In addition, peak-to-peak changes in C_m are higher for the two-bladed one during the start-up period (see Fig. 3.12a). As presented in Fig. 3.13a, for the two-bladed turbine 6 frequencies below 7 Hz seem to be separated from the others in terms of amplitude. For the three-bladed one there seems to be 3 dominant frequencies in 0 – 11 Hz range and in general the frequency spectrum is wider. Overall, it can be said that the three-bladed turbine shows better performance

during the start-up with more stable and less vibratory rotations. As the rotational speeds increase C_m curves shift to negative values more often resulting in a more vibratory behavior.

Figure 3.10b presents the responses of the turbines in the transition region obtained by letting the turbines rotate 1 cycle with *TSR* = 0.75, 1 and 1.5. Peak to peak amplitude changes for the two-bladed turbine are higher, suggesting more severe vibrations as shown in Fig. 3.12b. Although its mean values for whole transition region are higher, its RMS and standard deviation values are also higher than ones of the three-bladed turbine as seen in Fig. 3.11b. Two-bladed turbine has 5 dominant frequencies while three-bladed one has 6 with smaller amplitudes. It can be said that the two-bladed turbine performs better than three-bladed one in the transition region although it causes more fatigue loads on the blades.

Fig. 3.10c is obtained by rotating the turbines 2 cycles at their optimum *TSR* values, i.e. 2.5 and 3.5 for two- and three-bladed turbines, respectively. Although the two-bladed turbine can create higher instantaneous moment coefficients, as seen in Fig. 3.8 the overall C_m of the three-bladed one is higher at its optimum *TSR*. It is important to note that the three-bladed one almost never produces negative moments at its design *TSR*, which is not the case for the two-bladed one. The two-bladed turbine experiences short periods of decelerations during its operation at its optimum *TSR*. This is definitely not desired. In addition, peak-to-peak differences of two-bladed turbine are almost two times that of the three-bladed one as shown in Fig. 3.12c. It increases significantly the fatigue loads on the turbine blades. Also, there is only one dominant frequency for the three-bladed one while it is three for the other as seen in Fig. 3.13c. It is obviously seen that the three-bladed turbine performs better than two-bladed one.

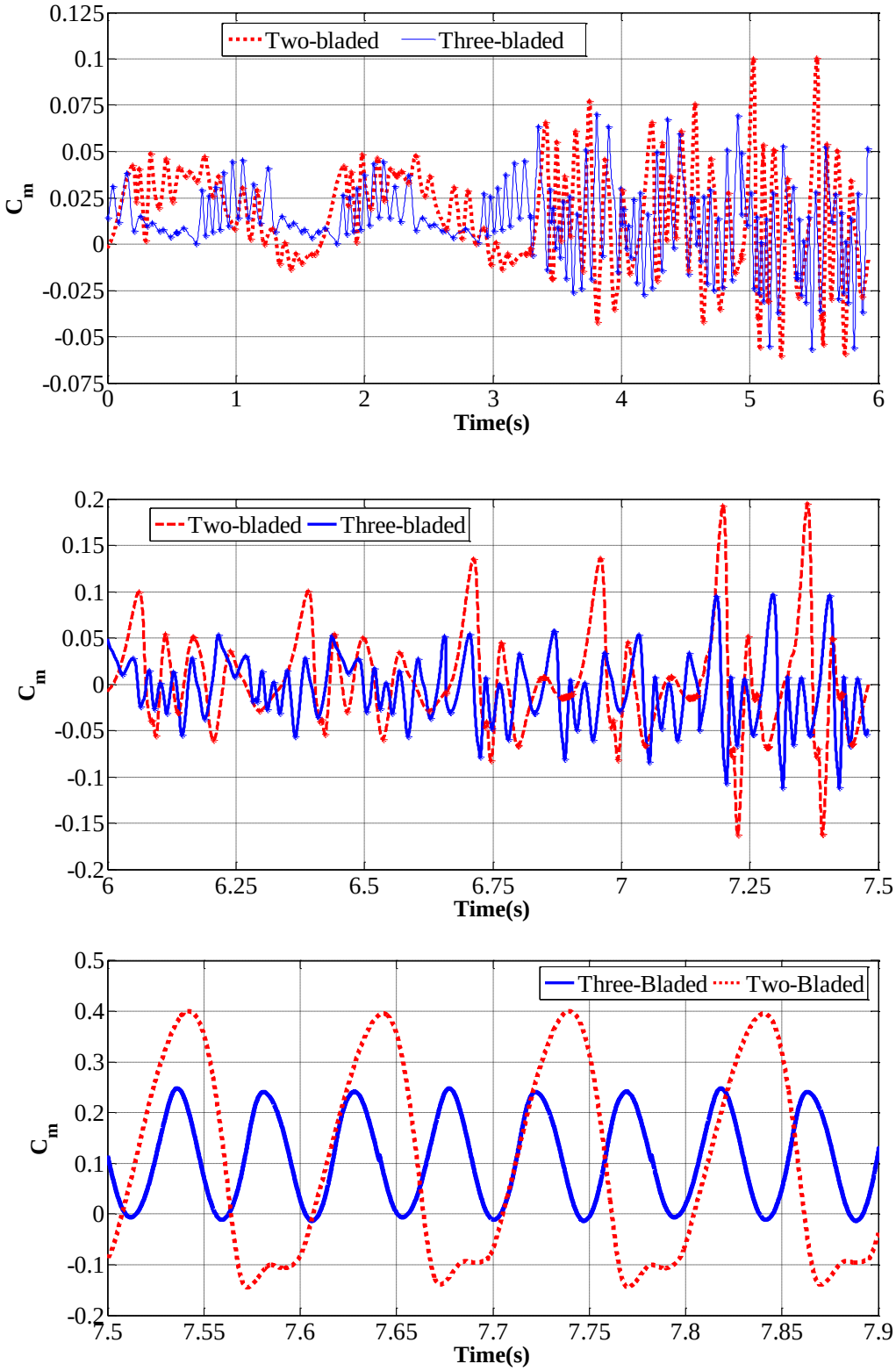

Figure 3.10. The start-up (top), transition (middle) and optimum (bottom) operation response of the moment coefficient for two- and three- bladed VAWTs

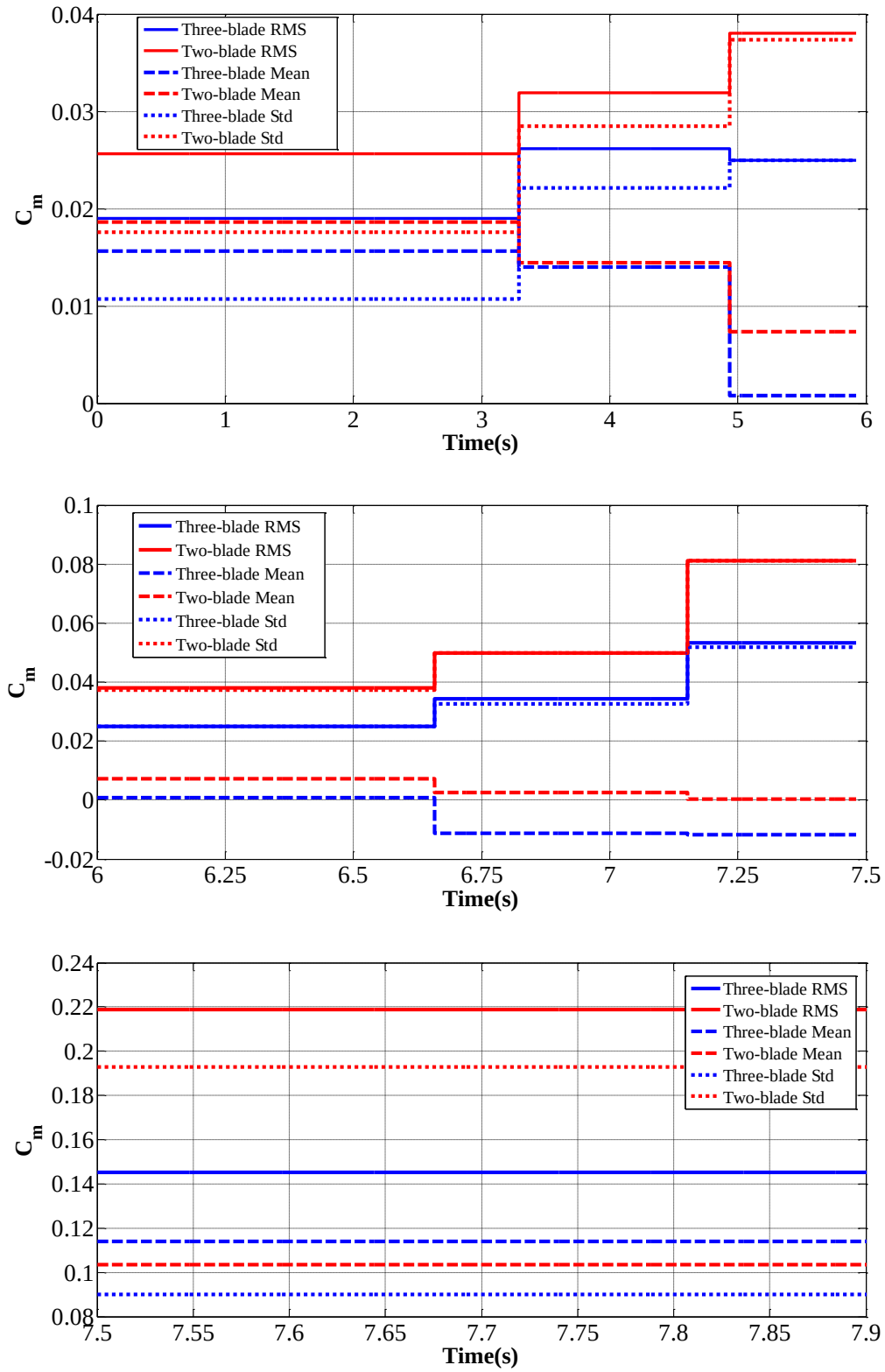

Figure 3.11. RMS, mean and standard deviation of the start-up (top), transition (middle) and optimum (bottom) operation responses for two- and three- bladed VAWTs

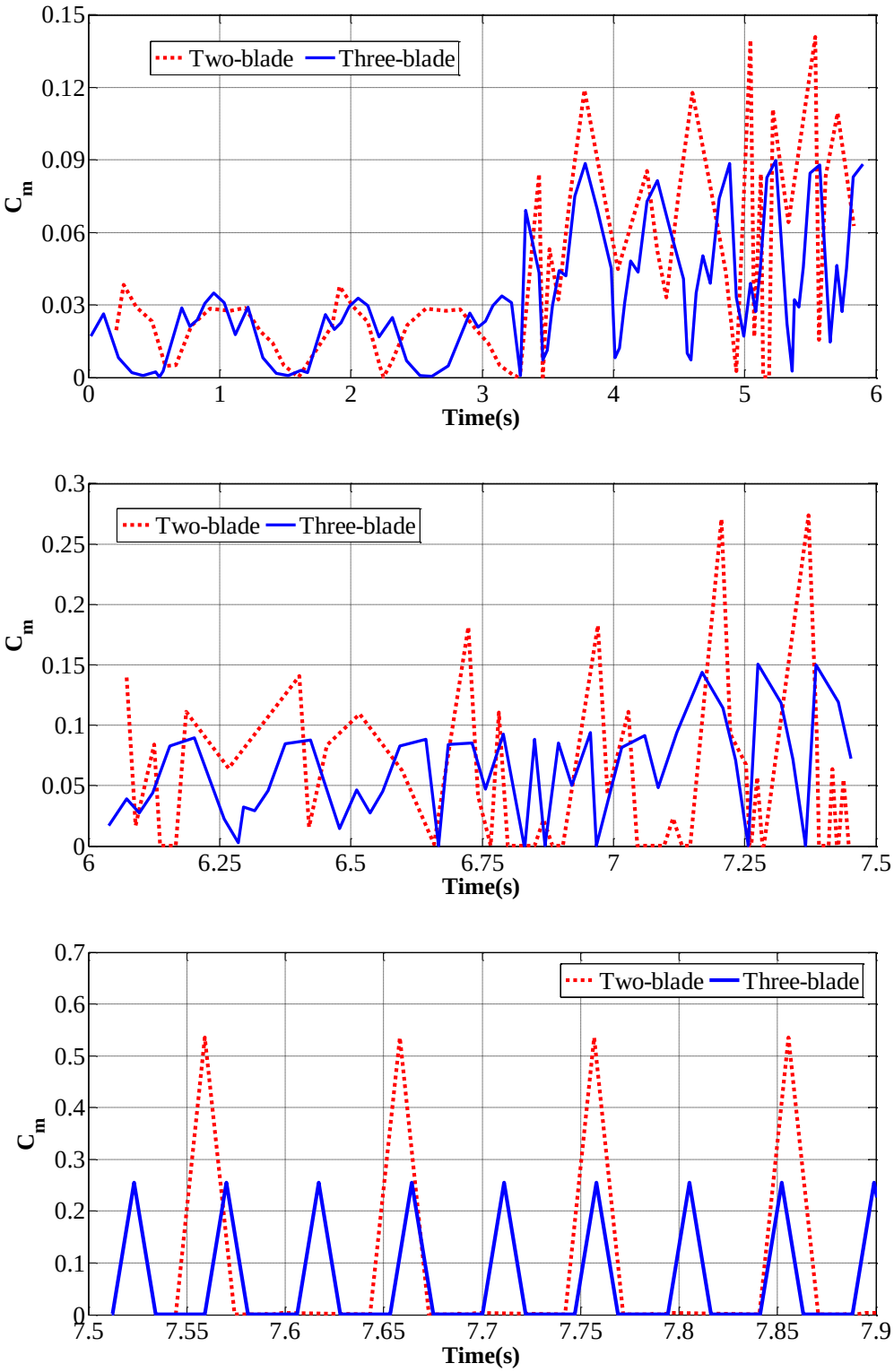

Figure 3.12. Peak-to-peak change of the start-up (top), transition (middle) and optimum (bottom) operation responses for two- and three- bladed VAWTs

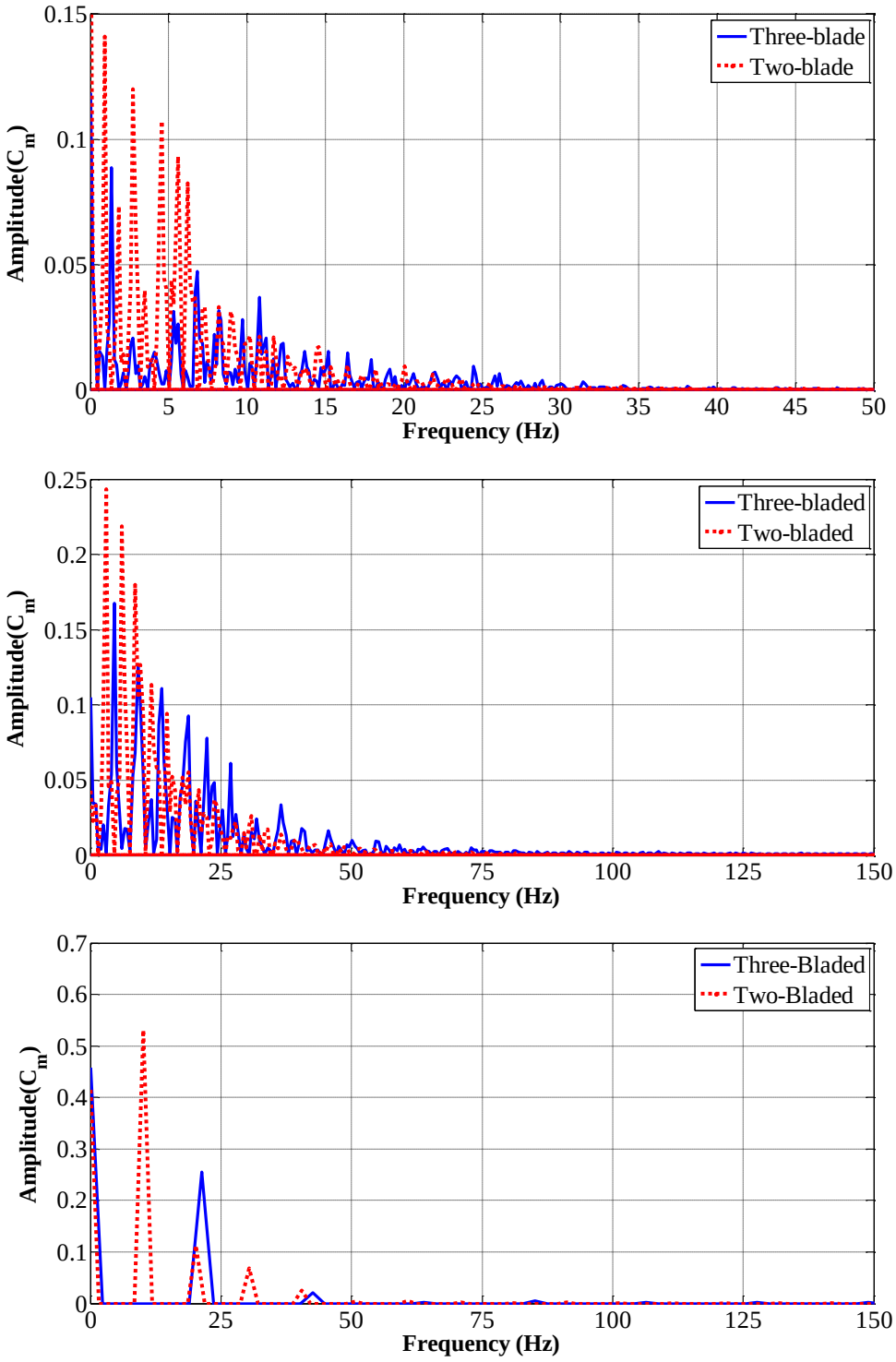

Figure 3.13.Absolute peak power spectrum of the start-up (top), transition (middle) and optimum (bottom) operation responses for two- and three- bladed VAWTs

Fig. 3.14 combines all three plots of Fig. 3.10 into a single one, showing the whole unsteady speed up for two- and three-bladed turbines separately. Overall moment coefficients pressure Overall moment coefficients at respective optimum TSR values of the turbines are also shown in the figure. Similar plots are given in Fig. 3.15 for the generated power. It is seen that the output of the turbines are very low until they reach their optimum rotational speeds. Start-up, transition and optimum operation regimes are easily recognized especially in the power variations.

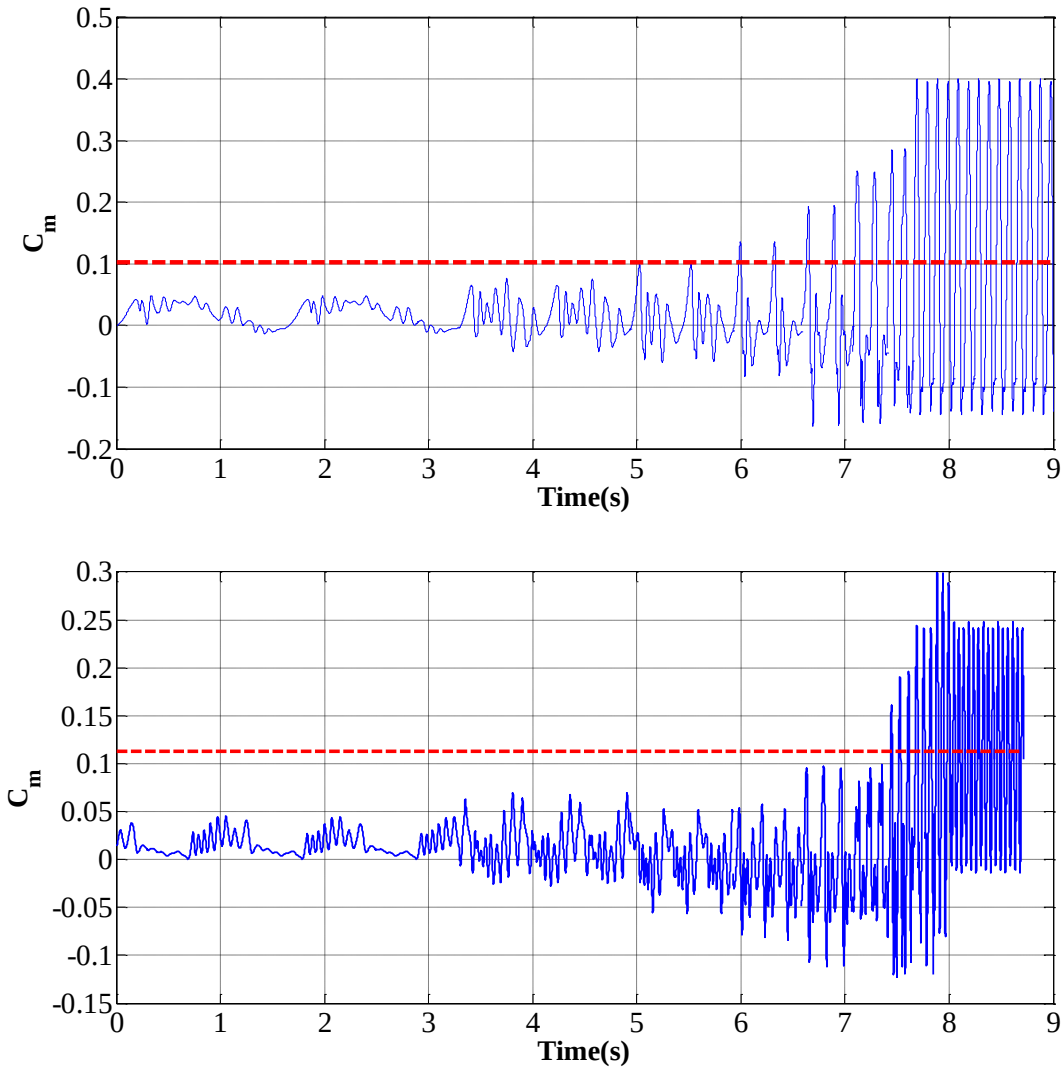

Figure 3.14. Unsteady and optimum mean response of the moment coefficient for two-bladed (top) and three-bladed (bottom) VAWTs

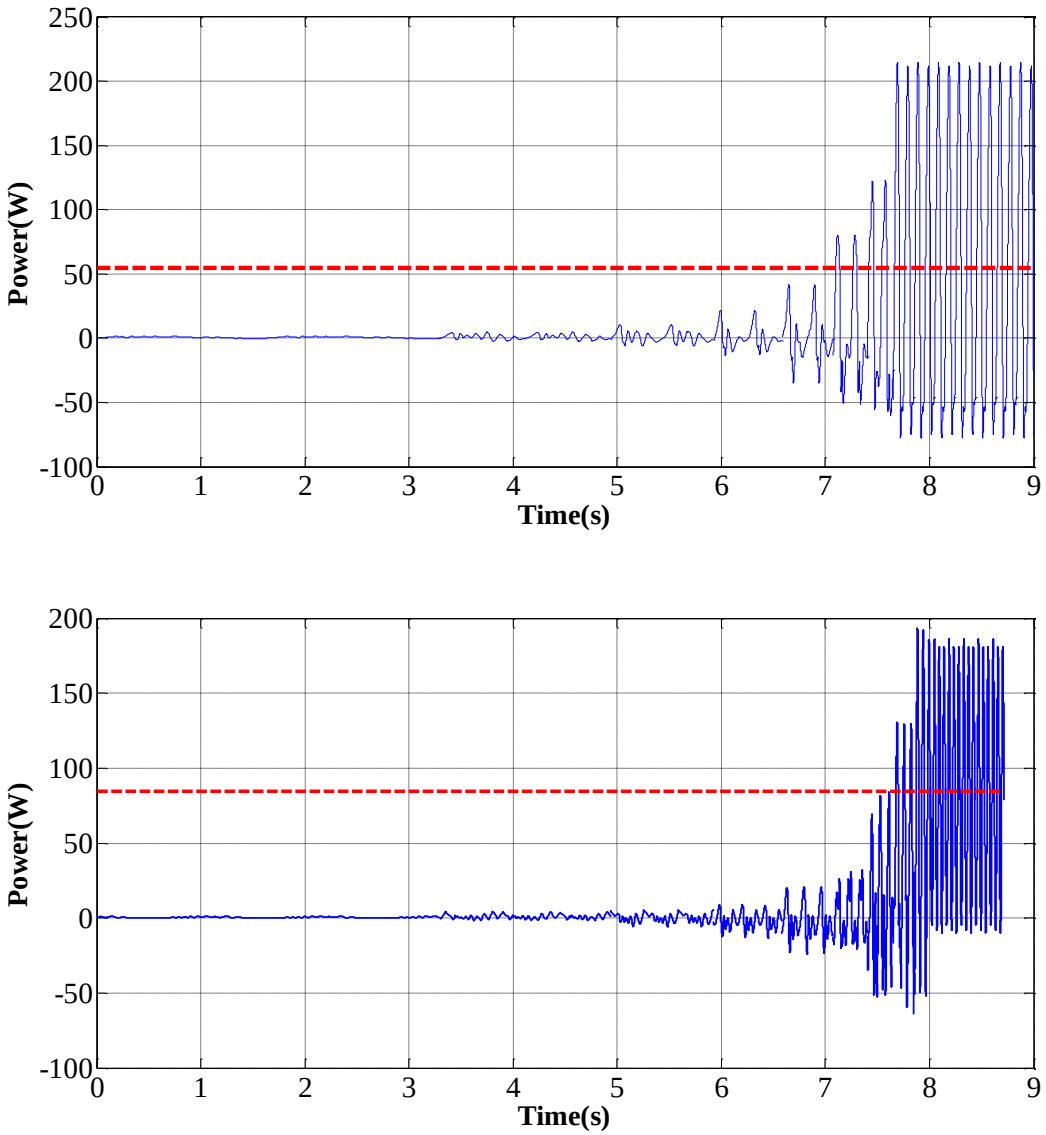

Figure 3.15. Unsteady and optimum mean response of the power output for two-bladed (top) and three-bladed (bottom) VAWTs

CHAPTER 4

SUMMARY and CONCLUSIONS

Performance of two- and three-bladed Darrieus type vertical axis wind turbines are studied using two-dimensional sliding mesh type CFD simulations. Blades are selected to be straight with NACA 0021 profile and 1 m height. Turbine diameter is set to be 1.1 m and at 7 m/s wind speed the turbine is expected to deliver 92.5 W maximum power output. Blade chord length is chosen to be 98 mm for the three-bladed configuration and to keep the solidity ratio fixed, it is increased to 147 mm for the two-bladed version. The origin of this thesis work goes back to the Teknogirisim Funding project supported by the Turkish Ministry of Science, Industry and Technology that the author worked on and most of the above mentioned selections were done during that study.

The completed work can be summarized in two parts. The first part consisted of independency simulations, in which mesh independency, time step independency and residual tolerance independency simulations are done. These are of upmost importance for a reliable numerical practice and accurate results, but in literature they are rarely reported appropriately. In this study considerable time is dedicated to these simulations. The most time consuming part was the generation of a proper mesh and performing the mesh independency study. First, an all unstructured mesh was tried, but mesh independent results could not be obtained. It was realized that without a carefully crafted structured boundary layer mesh, it is not possible to get acceptable results in an efficient way. After several trials, three levels of hybrid mesh all having structured boundary layer and unstructured outer regions were built and by comparing their unsteady moment coefficient results one of them was selected for future runs. Time step and residual tolerance tests were relatively simpler. It was seen that the default tolerance values suggested by ANSYS Fluent was not enough and lower values were selected. As the time step was reduced simulations, not

necessarily took longer time because of the increased stability and the need for less iterations to reach convergence in each time step.

In the second part of the thesis first the parameters that decided on with the help of the independency simulations were adapted for the actual simulations. In the independency simulations there were a single blade and a single rotational speed. New meshes are prepared for two- and three-bladed turbines and proper time steps are calculated for different rotational speeds, i.e. tip speed ratios (*TSR*). Simulations are done for 11 *TSR* values in the range 0.15 - 4.0. Variation of the moment coefficient during a full cycle of two- and three-bladed turbines are examined for all *TSR*s. Overall moment coefficient vs. *TSR* plots are generated for the two turbines and their start-up, transition and optimum operation ranges were determined. Finally unsteady speed up behavior of the turbines are roughly simulated by stitching discrete *TSR* simulations to each other.

Important conclusions are as follows

- During the simulations, meshes having the structured boundary layer elements around the blades should be used to decrease the solution time. To satisfy the same first layer heights as boundary layer elements, more and more triangular elements are needed and it cause significant increase in the solution time.
- When the first layer height of boundary layer mesh is too small, it may result in unstable solutions.
- The default convergence tolerance value (10^{-3}) of Fluent is inappropriate for 2D simulations of VAWTs.
- To overcome unstable solutions observed at small TSRs, either time step size or under-relaxation factors can be decreased.
- Smaller time step size reduces the number of iterations required at each time step.
- It is not easy to use second order discretizations since they need much finer meshes and smaller time steps for stable solutions.

- Compared to the two-bladed one, three-bladed turbine shows better start-up and transition characteristics with less vibrations due to higher possibility of blades being actively used in a cycle. This suggests that start-up and transition characteristics can be improved further by adding more blades. Of course this will also have an effect on the generated wake profiles and blade-to-blade interactions.
- Two-bladed turbine reaches its optimum operation at a smaller *TSR* than the three-bladed one. At their optimum operating points, efficiency of the three-bladed turbine is 13 % higher than that of the two- bladed one. These again suggest the trial of using more blades to see if the trends continue or not.
- To get more smooth rotations and electric generator outputs and to eliminate blade wake losses, one bladed turbine having spiral structure of 360° should be used. However, it can result in high manufacturing costs.
- Even with a multi-processor, multi-core high end workstation, unsteady sliding mesh simulations of 2D flows are time consuming. For 3D definitely more advanced parallel computing capabilities are necessary.
- To get the effect of blade tips, supporting struts and turbine shafts 3D simulations are needed. In other words, it is expected to obtain overestimations in overall turbine performances from 2D sliding mesh simulations.
- The positive influences of the blades are observed at the upwind region of the turbine while the negative ones are done at the downwind region. It is reasoned due the value and position of pressure fields on the turbine blades.

To finish, the following list of possible future work that can be used to improve the current study

- The turbine can be scaled up to get more practical power values, in the order of 1-5 kW.
- The effect of 2D simplification on the correctness of the results can be examined.
- Fluid structure interaction simulations can be done to understand the start-up behavior in a more physical manner.

- Turbines with more than three blades can be simulated if the trend of increased power with blade number continues or not. It is also important to see how this effects the start-up behavior.
- The effect of airfoil details such as camber, thickness, etc. on the power output can be studied. To guide these studies velocity and pressure contour plots should be studied in detail.

REFERENCES

[1] Roth J. ,2010, Wind Resource Assessment Handbook ,New York State : NYSERDA

[2] State Climate Office of North Carolina, Climate Education-Coriolis Effect, Retrieved from http://www.nc-climate.ncsu.edu/edu/k12/.coriolis (last accessed on 15.01.2014)

[3] Methew S. ,2006, Wind Energy: Fundementals, Recouce Analysis and Economics, Netherlands: Springer

[4] Vestergaard J. , Brandstrup L. and Goddart R.D. , 2004, "A Brief History of the Wind Turbine Industries in Denmark and the United States", Academy of International Business Conference Proceedings, pp.322-327

[5] Global Wind Energy Council, Global Cumulative Installed Wind Capacity, Retrieved from http://www.gwec.net/wp-content/uploads/2012/06/Global-Cumulative -Installed- Wind-Capacity- 1996-20122.jpg (last accessed on 15.01.2014)

[6] Global Wind Energy Council, 2012, Global Wind Report: Annual Market Update-2012, pp.60-61

[7] The Scientific Earth Conscientious, Sandia National Laboratories's Wind Energy Researcers, Retrieved from http://scientificearthconscientious6. wordpress.com/2012/07/31 (last accessed on 15.01.2014)

[8] Helix Wind Inc., Products, Retrieved from http://www.helixwind.com/en/product.php (last accessed on 15.01.2014)

[9] REM Enterprises Inc., Products, Retrieved from http://www.pacwind.remnet.com/ page3.html (last accessed on 15.01.2014)

[10] Aeolos Wind Energy Ltd., Products, Retrieved from http://www.windturbinestar.com/ products.html (last accessed on 15.01.2014)

[11] The Alternative Energy Info, VAWTs, Retrieved from http://www.alt-energy.info/wind-power/want-to-know-more-about-vertical-axis-wind-turbines (last accessed on 15.01.2014)

[12] The Archi Expo, Virtual Architecture Exhibition/Ropatec VAWTs, Retrieved from http://www.archiexpo.com/prod/ropatec/small-vertical-axis-wind-turbines-darrieus-rotor-62272-160029.html (last accessed on 12.05.2013)

[13] Claessens M.C., 2006, "The Design and Testing of Airfoils for Application in Small Vertical Axis Wind Turbines",Thesis(MSc), Delft Univerisity of Technology.

[14] Islam M.,2008, "Analysis of Fixed-Pitch Straight-Bladed VAWT with Asymmetric Airfoils", Thesis (PhD), University of Windsor

[15] Batista,N.C., Melicio,R., Matias,J. and Catalo,J.P.,"Vertical Axis Wind Turbine Performance Prediction: An Approach to the Multiple Stream Tube

Model",International Conference on Renewable Energies and Power Quality,Spain,28-30 March 2012,
[16] Beri H. and Yao Y.,2011,"Double Multiple Stream Tube Model and Numerical Analysis of Vertical Axis Wind Turbines", Journal of Energy and Power Engineering,3, pp. 262-270
[17] Saeidi D., Sedaghat A., Alamdari P. and Alemrajabi A.,"Aerodynamic Design and Economical Evaluation of Site Specific Small Vertical Axis Wind Turbine", Journal of Applied Energy 101 (2013): 765-775
[18] Goude A.,2012,"Fluid Mechanics of Vertical Axis Turbines: Simulations and Model Development", Acta Universitatis Upsaliensis
[19] Strickland J.H., Webster B.T. and Nguyen T., "A vortex model of the Darrieus turbine: an analytical and experimental study", Trans ASME, J Fluids Eng 1979;101:500–5.
[20] Ponta F.L. and Jacovkis P.M.,2001, "A vortex model for Darrieus turbine using finite element techniques", Renew Energy, 24:1–18.
[21] Wang L.B., Zhang L. and Zheng N.D.,2007, "A Potential Flow 2-D Vortex Panel Method: Applications to Vertical Axis Straight Blade Tidal Turbine", Energy Conversion and Management , pp.454-461
[22] Angle G.M., Pertl F.A., Clarke M.A. and Smith J.E.,"Lift Augmentation for Vertical Axis Wind Turbines", International Journal of Engineering, 4, pp. 430-442
[23] Islam M., David S.,Ting K. and Fartaj A.,2006,"Aerodynamic Models for Darrieus Type Straight Bladed Vertical Axis Wind Turbines" , Renewable and Sustainable Energy Reviews, Vol.12, pp. 1086-1109
[24] Dumitrescu H. and Cardos V.,2009,"A Free Wake Method for Vertical Axis Wind Turbine Performance Prediction", Roum. Sci. Techn. – Méc. Appl., Tome 54, No 2, P. 87–100
[25] Hirsch C. and Mandal A.C., 1987, "Cascade Theory for the Aerodynamic Performance of Darrieus Turbines", Wind Engineering Vol.11-3, pp. 164-175
[26] Islam M.,2008, "Analysis of Fixed-Pitch Straight-Bladed VAWT with Asymmetric Airfoils", Ph.D. Thesis, University of Windsor, Ontario, Canada
[27] Lain S. and Osorio C.,2010, "Simulation and Evaluation of a Straight-Bladed Darrieus Type Cross-Flow Marine Turbine", Journal of Scientific and Industrial Research,69,pp. 906-912
[28] Carrigan T.J. ,Dennis B.H. ,Han Z.X. and Wang B.P., 2012, "Aerodynamic Shape Optimization of a Vertical Axis Wind Turbine Using Differential Evolution ", ISRN Renewable Energy Vol.12
[29] Biadgo A.M.,Simonovic A.,Komarov D. and Stupar S.,2013,"Numerical and Analytical Investigation of Vertical Axis Wind Turbine", FME Transactions, 41, pp.49-58
[30] Castelli M.R., De Betta S. and Benini E.,2012, "Effect of Blade Number on a Straight Bladed Vertical Axis Darrieus Wind Turbine", World Academy of Science-Engineering and Technology, 61, pp. 305-311

[31] Howell R., Qin N., Edwards J. and Durrani N.,2010, ”Wind Tunnel and Numerical Study of a Small Vertical Axis Wind Turbine”, Renewable Energy, 35, pp.412-422
[32] Green Energy Solutions Inc., Vertical Wind Turbines, Retireved from http://masteringgreen.com/ges-vawt. html (last accessed on 15.01.2014)
[33] Archer C.L. and Jacobson,M.Z.,2003, “The Spatial and Temporal Distributions of U.S. Wind and Windpower at 80 m Derived from Measurements”, Journal of Geophysical Research,108, No.D9
[34] Islam M.,2008, “Analysis of Fixed-Pitch Straight-Bladed VAWT with Asymmetric Airfoils”, Ph.D. Thesis, University of Windsor, Ontario, Canada
[35] Graham H.Z.,Panther C.,Hubbel M.,Wilhelm J.,Angle J.M. and Smith J.E.,2009, “Airfoil Selection for a Straight Bladed Circulation Controlled Vertical Axis Wind Turbine”, Proceedings of the ASME 2009 3rd International Conference of Energy Sustainability, San Francisco,USA, July 19-23
[36] Castelli R.C., Englaro A. and Benini E.,2011, “The Darrieus Wind Turbine: Proposal for a New Performance Prediction Model Based on CFD”, Energy, 36, pp.4919-4934

APPENDIX A

VELOCITY CONTOURS FOR TWO-BLADED TURBINE AT *TSR* = 3.0

Position: 0°

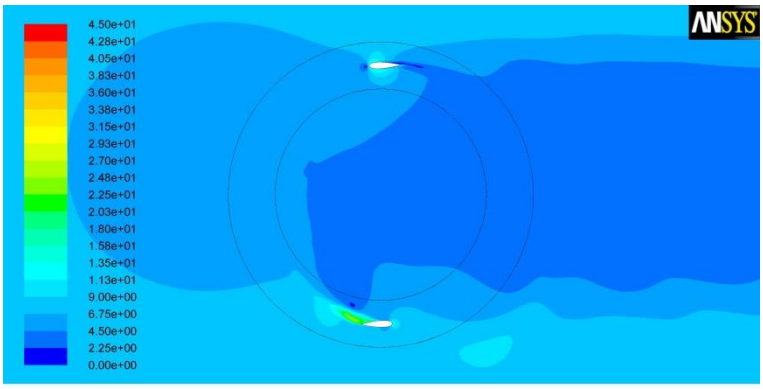

Position: 30°

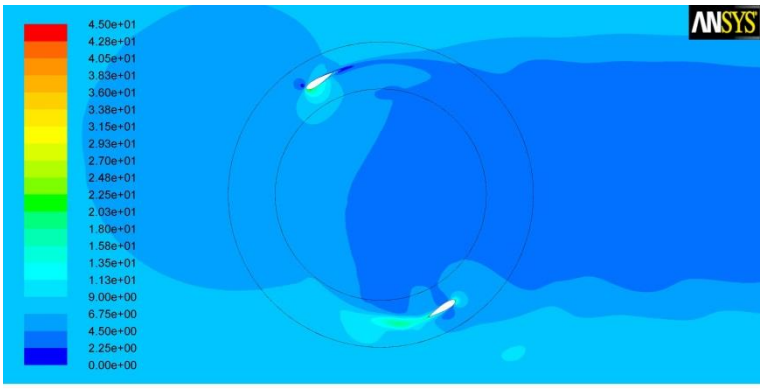

Position: 60°

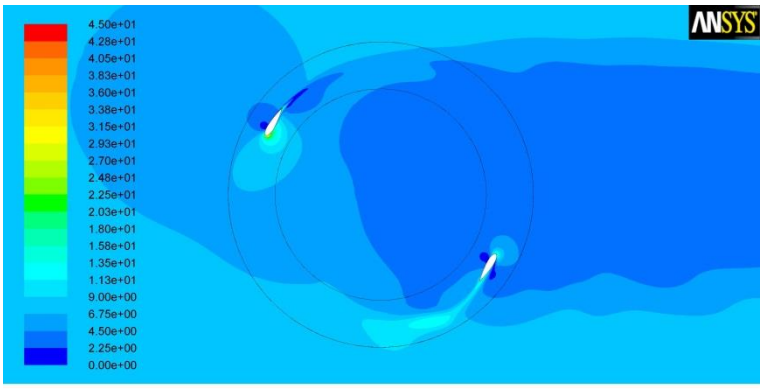

Position: 90°

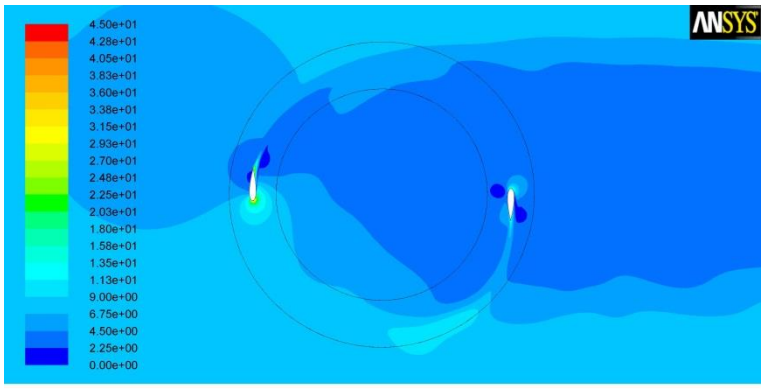

Contours of Velocity Magnitude (m/s) (Time=5.3446e-01)

Feb 18, 2014
ANSYS FLUENT 12.1 (2d, dp, pbns, skw, transient)

Position: 120°

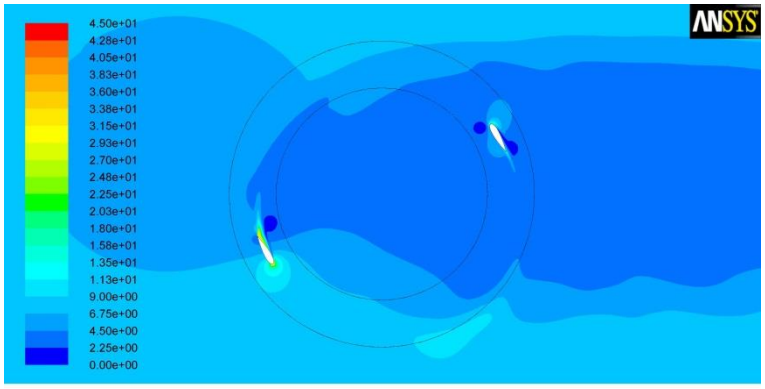

Contours of Velocity Magnitude (m/s) (Time=5.4816e-01)

Feb 18, 2014
ANSYS FLUENT 12.1 (2d, dp, pbns, skw, transient)

Position: 150°

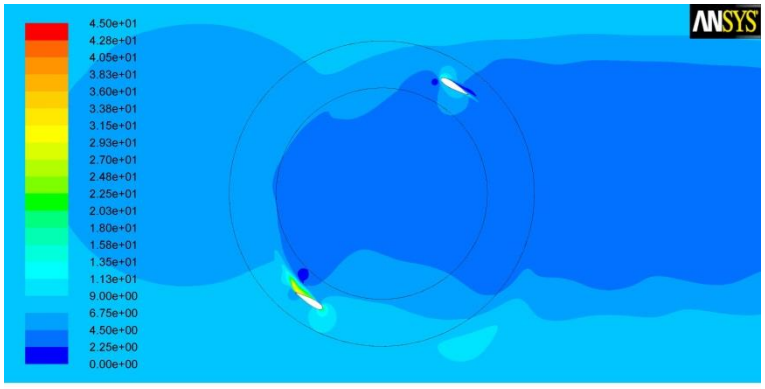

Contours of Velocity Magnitude (m/s) (Time=5.6186e-01)

Feb 18, 2014
ANSYS FLUENT 12.1 (2d, dp, pbns, skw, transient)

Position: 180°

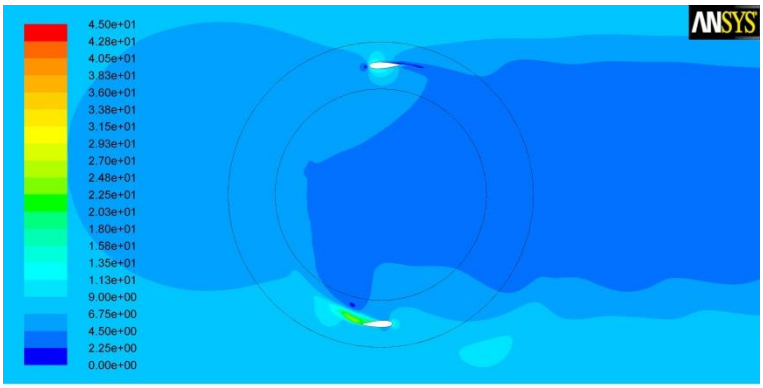

Contours of Velocity Magnitude (m/s) (Time=5.7671e-01)

Feb 18, 2014
ANSYS FLUENT 12.1 (2d, dp, pbns, skw, transient)

Position: 210°

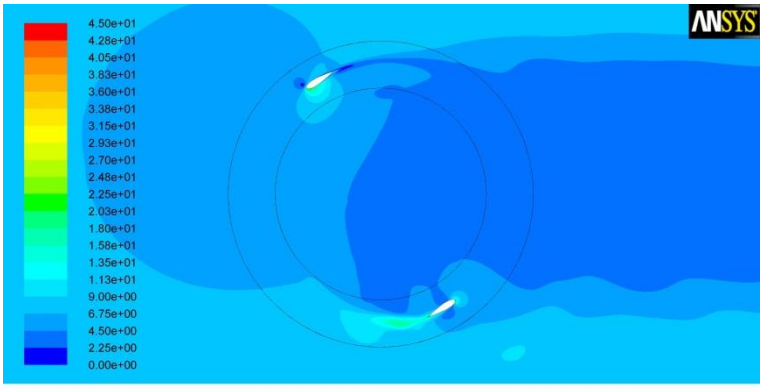

Contours of Velocity Magnitude (m/s) (Time=5.9041e-01)

Feb 18, 2014
ANSYS FLUENT 12.1 (2d, dp, pbns, skw, transient)

Position: 240°

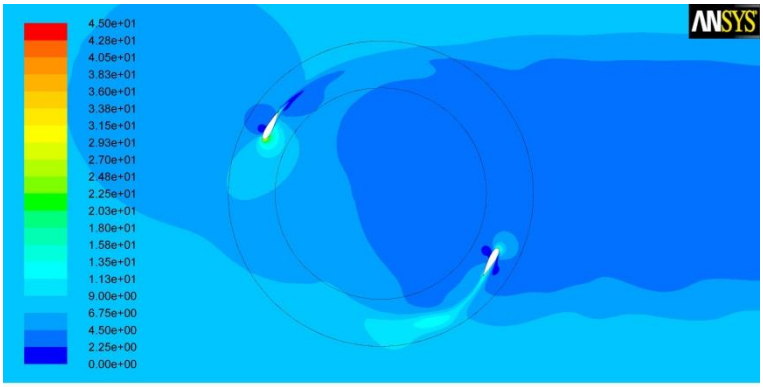

Contours of Velocity Magnitude (m/s) (Time=6.0412e-01)

Feb 18, 2014
ANSYS FLUENT 12.1 (2d, dp, pbns, skw, transient)

Position: 270°

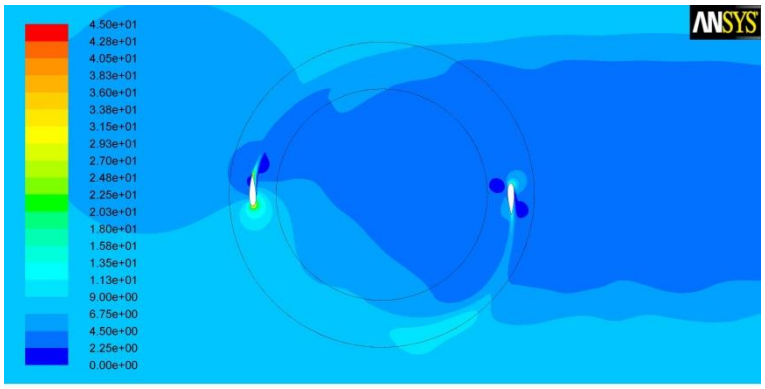

Contours of Velocity Magnitude (m/s) (Time=6.1782e-01)

Feb 18, 2014
ANSYS FLUENT 12.1 (2d, dp, pbns, skw, transient)

Position: 300°

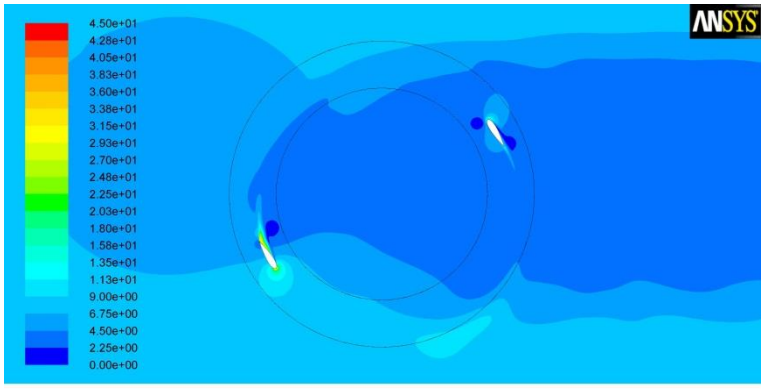

Contours of Velocity Magnitude (m/s) (Time=6.3153e-01)

Feb 18, 2014
ANSYS FLUENT 12.1 (2d, dp, pbns, skw, transient)

Position: 330°

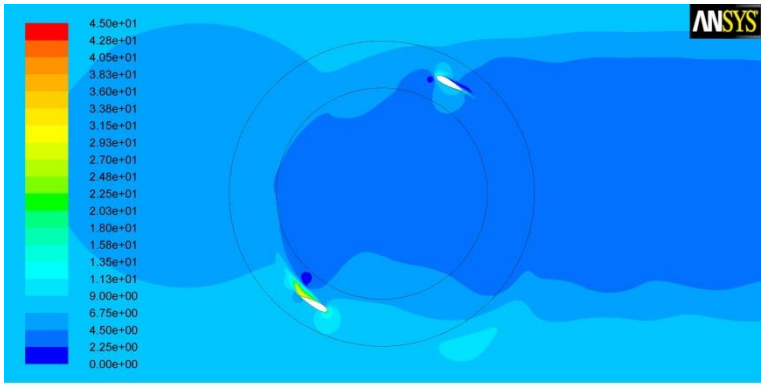

Contours of Velocity Magnitude (m/s) (Time=6.4523e-01)

Feb 18, 2014
ANSYS FLUENT 12.1 (2d, dp, pbns, skw, transient)

APPENDIX B

PRESSURE CONTOURS FOR TWO-BLADED TURBINE AT *TSR* = 3.0

Position: 0°

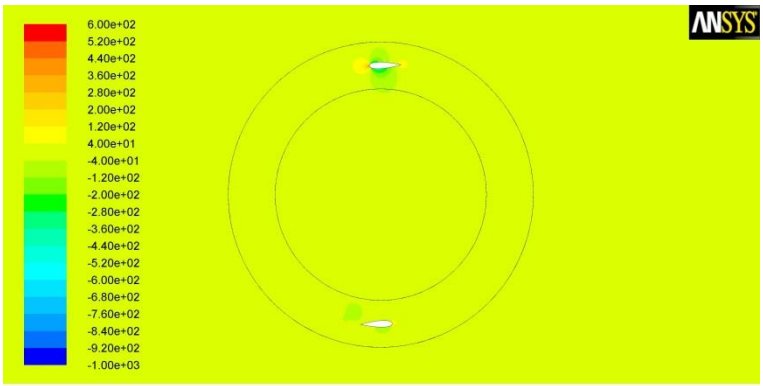

Contours of Static Pressure (pascal) (Time=5.7671e-01)

Feb 18, 2014
ANSYS FLUENT 12.1 (2d, dp, pbns, skw, transient)

Position: 30°

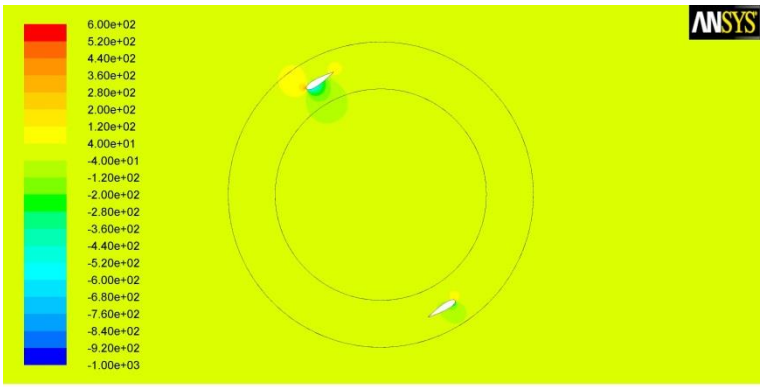

Contours of Static Pressure (pascal) (Time=5.9041e-01)

Feb 18, 2014
ANSYS FLUENT 12.1 (2d, dp, pbns, skw, transient)

Position: 60°

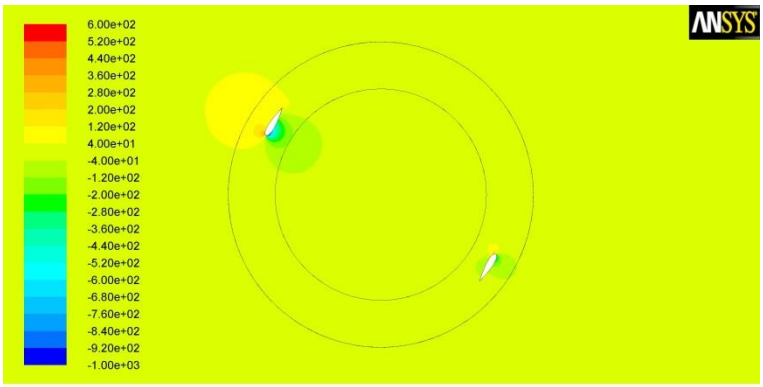

Contours of Static Pressure (pascal) (Time=5.2075e-01)

Feb 18, 2014
ANSYS FLUENT 12.1 (2d, dp, pbns, skw, transient)

Position: 90°

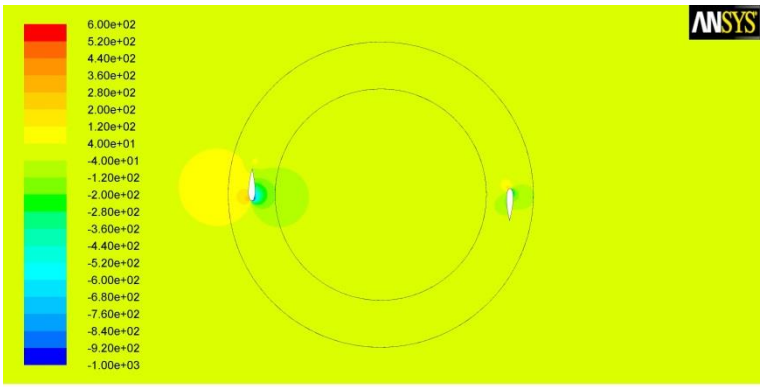

Contours of Static Pressure (pascal) (Time=5.3446e-01)

Feb 18, 2014
ANSYS FLUENT 12.1 (2d, dp, pbns, skw, transient)

Position: 120°

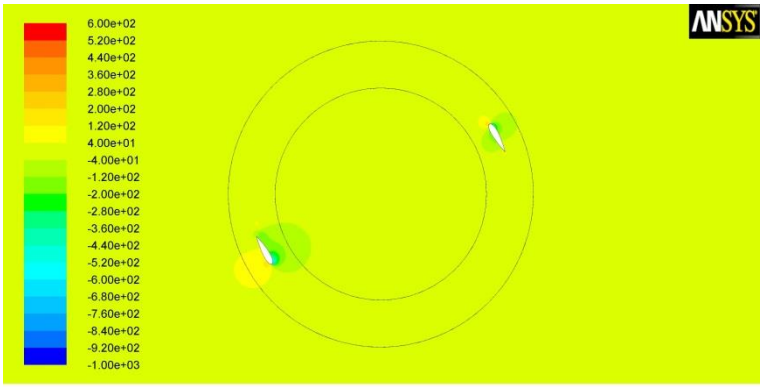

Contours of Static Pressure (pascal) (Time=5.4816e-01)

Feb 18, 2014
ANSYS FLUENT 12.1 (2d, dp, pbns, skw, transient)

Position: 150°

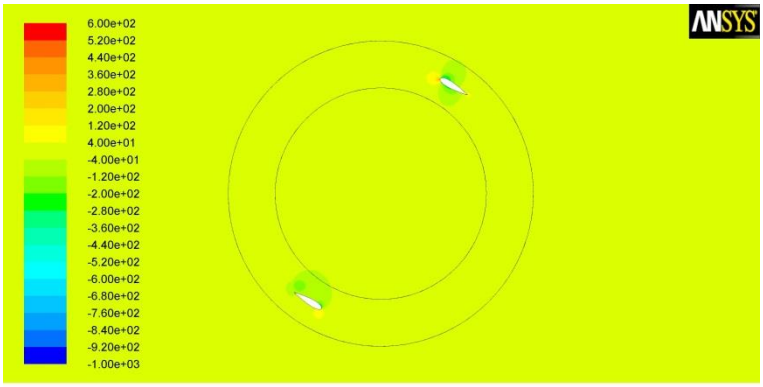

Contours of Static Pressure (pascal) (Time=5.6186e-01)

Feb 18, 2014
ANSYS FLUENT 12.1 (2d, dp, pbns, skw, transient)

Position: 180°

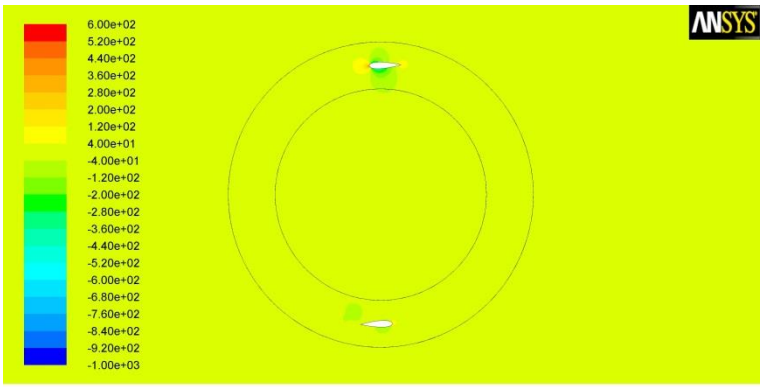

Contours of Static Pressure (pascal) (Time=5.7671e-01)

Feb 18, 2014
ANSYS FLUENT 12.1 (2d, dp, pbns, skw, transient)

Position: 210°

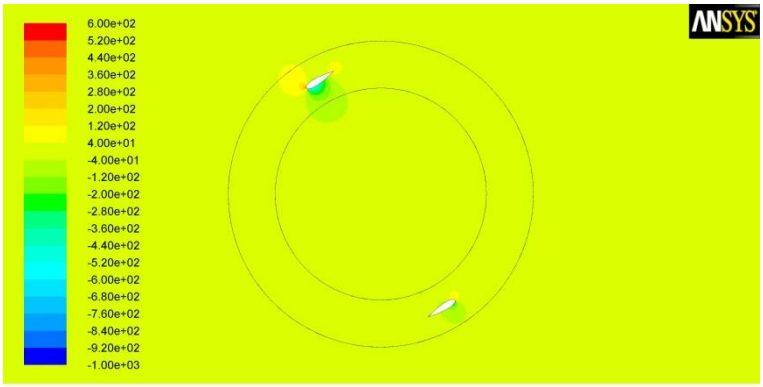

Contours of Static Pressure (pascal) (Time=5.9041e-01)

Feb 18, 2014
ANSYS FLUENT 12.1 (2d, dp, pbns, skw, transient)

Position: 240°

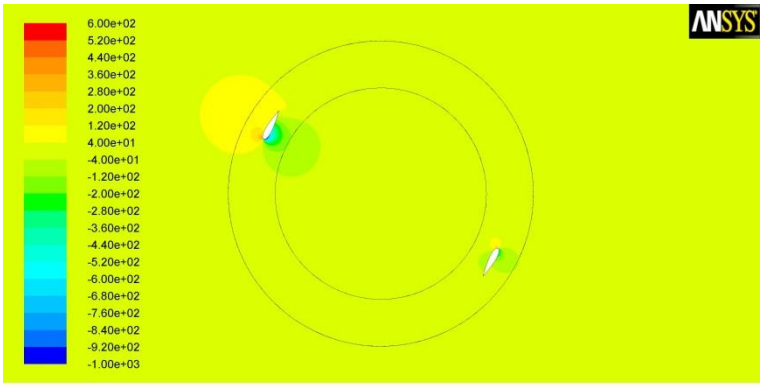

Contours of Static Pressure (pascal) (Time=6.0412e-01)

Feb 18, 2014
ANSYS FLUENT 12.1 (2d, dp, pbns, skw, transient)

Position: 270°

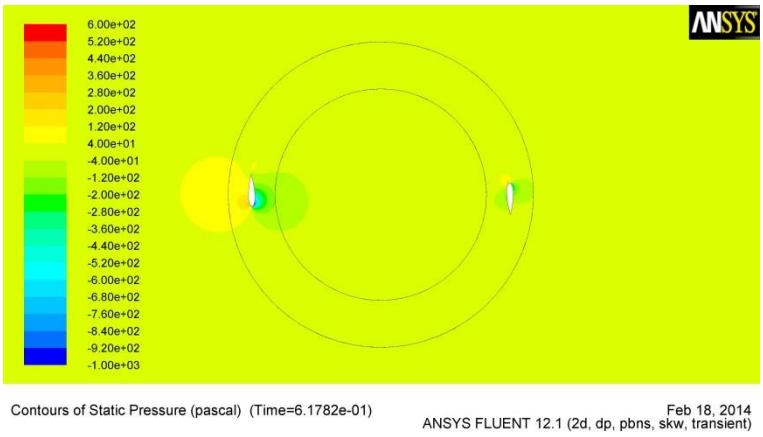

Contours of Static Pressure (pascal) (Time=6.1782e-01)

Feb 18, 2014
ANSYS FLUENT 12.1 (2d, dp, pbns, skw, transient)

Position: 300°

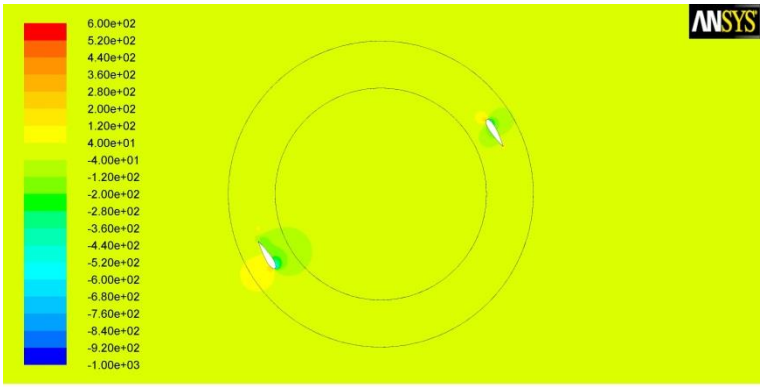

Contours of Static Pressure (pascal) (Time=6.3153e-01)

Feb 18, 2014
ANSYS FLUENT 12.1 (2d, dp, pbns, skw, transient)

Position: 330°

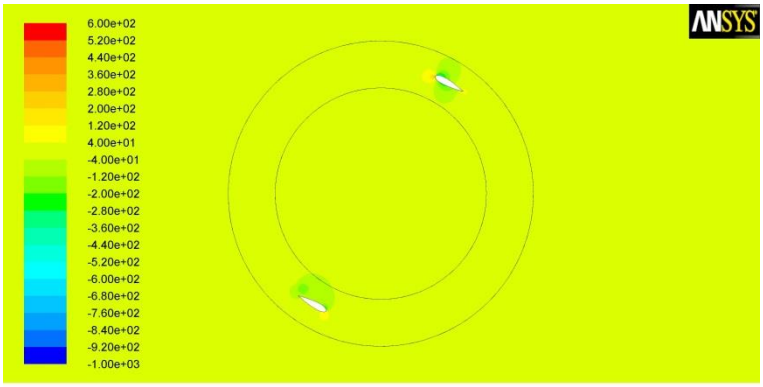

Contours of Static Pressure (pascal) (Time=6.4523e-01)

Feb 18, 2014
ANSYS FLUENT 12.1 (2d, dp, pbns, skw, transient)